Point-Based Manifold Harmonics

Yang Liu, Balakrishnan Prabhakaran, Xiaohu Guo

Abstract—This paper proposes an algorithm to build a set of orthogonal Point-Based Manifold Harmonic Bases (PB-MHB) for spectral analysis over point-sampled manifold surfaces. To ensure that PB-MHB are orthogonal to each other, it is necessary to have symmetrizable discrete Laplace-Beltrami Operator (LBO) over the surfaces. Existing converging discrete LBO for point clouds, as proposed by Belkin *et al* [1], is not guaranteed to be symmetrizable. We build a new point-wisely discrete LBO over the point-sampled surface that is guaranteed to be symmetrizable, and prove its convergence. By solving the eigen problem related to the new operator, we define a set of orthogonal bases over the point cloud. Experiments show that the new operator is converging better than other symmetrizable discrete Laplacian operators (such as graph Laplacian) defined on point-sampled surfaces, and can provide orthogonal bases for further spectral geometric analysis and processing tasks.

Index Terms—Point-Sampled Surface, Laplace-Beltrami Operator, Eigen Function

1 Introduction

1.1 Background

In computer image processing, spectral methods like Discrete Cosine Transform and Discrete Fourier Transform are widely used for analyzing signals. But these techniques do not work on geometric processing. One difficulty of applying spectral techniques on geometric processing is defining a set of suitable bases. The eigen-functions of Laplace-Beltrami Operator could serve this purpose.

Laplace operator Δ is a simple second-order differential operator (the divergence of gradient) defined in Euclidean space $\mathbb{R}^n$. Similarly, we can define Laplace-Beltrami Operator (LBO) in the compact boundaryless n-dimensional orientable Riemannian manifold $\mathcal{M}$ as the divergence of gradient:

$$\Delta_{\mathcal{M}} f = \operatorname{div} \operatorname{grad} f. \tag{1.1}$$

The eigen problem of LBO can be defined as:

$$\Delta_{\mathcal{M}} H = -\lambda H, \tag{1.2}$$

where λ and H are the eigen-value and corresponding eigen-function (eigen-vector in discrete form). Here the minus sign "-" is used to ensure that all $\lambda \geq 0$. Note that some researchers [2] define $\Delta_{\mathcal{M}} = -\operatorname{div} \operatorname{grad}$, in which case the minus sign in equation (1.2) can be removed. From now on we will denote the i-th eigen-value and the corresponding eigen-function (eigen-vector) as λ_i and H^i.

LBO is a symmetric operator in compact boundaryless orientable manifold [3]:

$$< f, \Delta_{\mathcal{M}} g > = \int_{\mathcal{M}} f \cdot \Delta_{\mathcal{M}} g \tag{1.3}$$

$$= - \int_{\mathcal{M}} < \nabla f, \nabla g > \tag{1.4}$$

$$=< \Delta_{\mathcal{M}} f, g > . \tag{1.5}$$

Here f and g are functions defined over the manifold surface, ∇ denotes the gradient operator. With this property, we know that eigen-functions with different eigen-values are orthogonal to each other:

$$< H^i, \Delta_{\mathcal{M}} H^j >= \lambda_j < H^i, H^j > \tag{1.6}$$

$$= < \Delta_{\mathcal{M}} H^i, H^j >= \lambda_i < H^i, H^j > \tag{1.7}$$

$$\text{if } \lambda_i \neq \lambda_j \text{ then} \tag{1.8}$$

$$< H^i, H^j >= 0. \tag{1.9}$$

Note that constant functions with $\lambda = 0$ is a solution for any Laplacian operator. We denote $\lambda_0 = 0$ with corresponding eigen-function $H^0 = constant$. Other eigen-values are sorted according to their magnitudes: $0 = \lambda_0 \leq \lambda_1 \leq \lambda_2 \leq \cdots$.

With the development of 3D scanning technology, it is much easier to generate 3D models from real objects today. For most of these surfaces we only have discrete representations such as polygonal meshes or point clouds. Thus we need to define the discrete form of LBO over the discrete representation of surfaces to perform the geometric analysis. By solving the above eigen problem, we can get a set of eigen-values $\{\lambda_i\}$ and corresponding eigen-vectors $\{H^i\}$ defined over the discrete manifold surfaces [4]. Reuter *et al* [4] proposed to extract data of the manifold such as volume, boundary length and genus number using the eigen-values of LBO. The eigen-vectors are called the Manifold Harmonic Bases (MHB). They are intrinsic properties of the surface [4], [1] and have been used for spectral analysis over triangle mesh surfaces [5], salient feature extraction [6], and

Y. Liu, B. Prabhakaran and X. Guo are with the Department of Computer Science, University of Texas at Dallas, Richardson, TX, 75080 USA e-mail: {yxl072100, bprabhakaran, xguo}@utdallas.edu

many other applications [7]. These techniques further motivated some researches on image processing by reinterpreting an image as a Riemannian manifold [8].

1.2 Motivation and Contribution

As a discrete representation of surfaces, the point cloud is less explored, comparing with polygonal meshes. The 3D scanning devices can produce point clouds sampled from object surfaces easily. Comparing with mesh, point clouds do not provide any information about the connectivity. This makes point clouds more difficult to process than meshes. Because the Laplacian operator employed in Manifold Harmonics proposed by Vallet *et al* [5] requires the mesh connectivity information, it can not be applied to point clouds directly. This paper extends the Manifold Harmonics framework to the geometry processing of point clouds.

Belkin *et al* [1] proposed a novel method to compute the discrete LBO on manifolds represented by point clouds. They also proved that this discrete LBO denoted as L_P^t is converging as points get denser. Here convergence of L_P^t means that $L_P^t\mathbf{f}$ is converging to $\Delta_{\mathcal{M}} f$ point-wisely where $\mathbf{f}$ is the discrete form of function f. This property is called consistency in works related to finite element methods [9]. However, their discrete LBO is not guaranteed to be symmetrizable matrix. A matrix A is called *symmetrizable* [10] if it could be expressed as product of two symmetric matrices one of which is positive-definite. It is also called self-adjoint matrix with respect to a given inner product. It is obvious that any symmetric matrix is also symmetrizable. Because LBO is symmetric, discrete LBO is expected to be symmetrizable matrix. It is important for discrete LBO to be symmetrizable in Manifold Harmonics because symmetrizable matrix operator is guaranteed to provide orthogonal bases. For discrete LBO matrix L, if it can be decomposed as $L = B^{-1}Q$ where Q is symmetric and B is symmetric positive-definite, it is a widely-used technique to compute the generalized eigen problem $Qx = -\lambda Bx$ instead of the standard eigen problem $Lx = -\lambda x$ [4]. With a modified definition of inner product $< x, y >= x^T By$, it is possible to ensure orthogonality of the eigen-vectors. But this technique is not applicable to L_P^t, which is explained in section 3.5. Using $(L_P^t + (L_P^t)^T)/2$ instead of L_P^t is a trivial extension to make it symmetrizable. Lévy [11] used this technique with cotangent weighted graph Laplacian. But our experiments in section 5 show that this trivial extension does not converge. Any technique to make L symmetrizable that modifies L_P^t itself will invalidate the convergence proof. Because we want our method to be geometry-aware, this is not acceptable either.

To ensure that the bases $\{H^i\}$ are orthogonal to each other, we propose a new method to construct the symmetrizable discrete LBO $\hat{L}_P^t$ over point clouds sampled from manifold surfaces. We also prove that this new operator is converging when point clouds get denser and satisfy certain sampling conditions. Based on the symmetrizable property of this new operator, we can construct a set of point-wisely converging manifold harmonic bases, to be used for general spectral analysis over the point-sampled surfaces. We summarize the contributions of this paper as follows:

1) We propose a provable construction algorithm for the *symmetrizable* and *converging* discrete Laplace-Beltrami operator over point-sampled manifold surfaces based on computing the integration over the manifolds numerically. The symmetrizable property of the discrete LBO, resulted from our local Voronoi computation, guarantees the orthogonality of the computed Point-Based Manifold Harmonic Bases (PB-MHB). The construction process based on the heat diffusion kernel guarantees the convergence of the discretized LBO (Theorem 4.2), and leads to more accurate manifold harmonic bases.
2) Our algorithm can be directly applied to the point clouds using a local Voronoi computation procedure in the tangential space, based on our theoretical proof that the estimated Voronoi cell area on the tangential space is converging to its counterpart on the manifold (Theorem 4.1), as long as the point clouds satisfy certain sampling condition (addressed in section 3.2). So we do not need a global mesh for the manifold surface to compute the orthogonal bases.
3) The experimental results shown in section 5 are very encouraging. The convergence of our new LBO is better than other point-based symmetrizable discrete Laplace operators, such as the graph Laplacian, Kirchhoff Laplacian, or the trivial extension of Belkin *et al*'s discrete operator $(L_P^t + (L_P^t)^T)/2$. The computed orthogonal bases are fully geometry-aware, and are performing better than those operators for general geometric processing tasks such as spectral filtering and feature extraction.

2 Related Work

Researchers have been looking for spectral geometric processing methods [7], [12], for surface smoothing [13], segmentation [14], compression [15], watermarking [16], [17], quadrangulation [18], [19], conformal parameterization [20], matching and retrieval [4], [6], etc. Manifold Harmonics, as proposed by Vallet *et al* [5], is defined as the eigen-functions of LBO, based on the Discrete Exterior Calculus (DEC) computational framework.

Discretizing Laplacian operator on mesh surfaces is an active research area. Most of the proposed discretization methods [13], [21], [22], [23] applied

finite element methods (FEM) with different assumptions. They have similar forms of *cotangent scheme* [24] despite those different assumptions. Xu [23] gave a theoretical analysis of the available discrete LBOs defined on meshes about their convergence property. It shows that the cotangent scheme does not converge to the continuous counterpart in general, except for the versions in Desbrun *et al* [21] and Meyer *et al* [22] applied to some special classes of meshes, such as certain meshes with valence 6. Hildebrandt *et al* [25] analyzed the convergence of LBO and showed that the cotangent scheme has weak convergence for the solution of the Dirichlet's problem, assuming the aspect ratios of the triangles are bounded. A recent work by Wardetzky *et al* [26] showed that a "perfect" discrete LBO based on mesh connectivity satisfying all the properties of the continuous one cannot exist on general meshes under certain restrictions such as piecewise linear functions. Reuter *et al* [27] showed that their discrete LBO based on cubic FEM works very well with respect to the continuous case, and demonstrated the applications in shape understanding. Peinecke *et al* [8] first proposed to use the spectrum of eigen-values as fingerprint for image recognition.

It is known that LBO and the heat equation on manifolds are closely related [2]. Belkin *et al* [28] extended this by proving that it is possible to approximate LBO on the estimated tangent planes of surfaces with the Gaussian kernel. They [29] proposed the first algorithm for approximating LBO of a surface from a mesh with point-wise convergence guarantees. Dey *et al* [30] proved the convergence of its eigen-values. This method was extended later [1] to discretize LBO on manifold surfaces represented as point clouds. Their matrix form LBO [1], denoted as L_p^t, has been proved to converge point-wisely as point clouds get denser. However, their discrete LBO on the point cloud is not guaranteed to be symmetrizable. So it cannot be used for computing the orthogonal bases on surfaces. LBO is naturally related to diffusion [31], which is also used in dimensional reduction and other applications.

Due to the lack of connectivity information, computing LBO on the point cloud is traditionally carried out in the local neighborhood of each point, by the combinatorial graph Laplacian [32], [16], which is hard to be geometry-aware. Since LBO is a differential operator, computing LBO on the point cloud is closely related to the integral computation on point clouds. Luo *et al* [33] worked on integral estimation over manifolds represented by point clouds. They employed the Voronoi diagrams based on the geodesic distance while our paper uses the Euclidean distance. We choose Euclidean Voronoi diagrams because it provides (1) the convergence rate of $O(\varepsilon^2)$ rather than $O(\varepsilon)$ of geodesic Voronoi diagrams, with the specific sampling condition ε defined in definition 3.1; and (2) bounding properties on both Voronoi cells and Voronoi neighbors that ease the proof of the final convergence property of our discrete LBO in Theorem 4.2. We estimate the area of the Euclidean Voronoi cell on the local tangent plane, and prove its convergence in Theorem 4.1. The proofs of the theorems are provided in the supplementary appendices. The convergence proof of the discrete LBO is dependent on some geometric properties of point clouds, e.g. sampling conditions, local feature size, etc., studied in the literature of surface reconstruction and computational geometry [34], [35].

3 Construction of PB-MHB

3.1 Overview

To construct PB-MHB, discrete LBO is necessary. Instead of discretizing LBO directly like finite element method, we discretize the integration of certain continuous functions defined over manifold which is proved to approximate $\Delta_{\mathcal{M}}$ (Lemma 5 in [28], Lemma 2.5 in Supplemental Appendices):

$$\Delta_{\mathcal{M}} f(p) = \lim_{t\to 0} \frac{1}{4\pi t^2}\Big(\int_{\mathcal{M}} e^{-\frac{\|p-y\|^2}{4t}} f(p) d\mu_y - \int_{\mathcal{M}} e^{-\frac{\|p-y\|^2}{4t}} f(y) d\mu_y\Big).$$

In section 3.2 several necessary definitions are introduced. In section 3.3 for each vertex p in the point cloud P, we discretize the integration mentioned above to approximate $\Delta_{\mathcal{M}} f(p)$ where f is a function defined over $\mathcal{M}$. In section 3.4 by representing this discretization in the form of matrix, we get our discrete LBO $\hat{\Delta}_P^t$.

In section 3.5 we compare our discrete LBO and Belkin's work to show why Belkin's work is not suitable for this case. In section 3.6 we show that the eigen-vectors of our discrete LBO, i.e. PB-MHB, are orthogonal to each other with respect to certain inner product, so PB-MHB can be used for spectral analysis.

3.2 Definitions

To construct the discrete LBO, the point clouds need to satisfy some sampling conditions defined as follows:

***Definition** 3.1 (Sampling Condition):* Let $\varepsilon > 0$. A finite sample $P \subset \mathcal{M}$ is called an ε-sample if

$$\forall x \in \mathcal{M}, \exists p \in P : \|x - p\| \leq \varepsilon. \tag{3.1}$$

And the ε-sample P is called an (ε, ζ)-sample or tight ε-sample if it satisfies the additional condition:

$$\forall p, q \in P : \|p - q\| \geq \zeta, \tag{3.2}$$

where $\varepsilon > \zeta > 0$.

It is obvious that any (ε, ζ)-sample is also an ε-sample.

In this paper, we assumed that the given point cloud P is an $(\varepsilon, s\varepsilon)$-sample of the manifold $\mathcal{M}$. $0 < s < 1$ is a fixed positive number for the given point cloud P. That is, any two points in P can not be extremely close. This property is used to ensure that

the estimation of the Voronoi cells described in section 3.3 is converging, which is Theorem 4.1. We will employ Voronoi cells on manifolds in the construction process of discrete LBO. The Voronoi cell of a point p on manifold is the intersection of $\mathcal{M}$ and the Voronoi cell of p in Euclidean space $\mathbb{R}^3$. We define the Voronoi cells on manifolds as follows:

***Definition** 3.2 (Voronoi Cell):* For the point set P sampled on the manifold $\mathcal{M}$, the Voronoi cell of a point $p \in P$ on $\mathcal{M}$ is defined as the subset of $\mathcal{M}$:

$$Vr_{\mathcal{M}}(p) = \{q | q \in \mathcal{M}, \forall p' \in P, p' \neq p, \|q-p\| \leq \|q-p'\|\},$$

where $\|q-p\|$ stands for the Euclidean distance between points p and q.

We also need to use the Local Feature Size to characterize how much the manifold $\mathcal{M}$ bends locally at a given point. The larger the feature size, the flatter the surface is. Local Feature Size is used by the theorems in section 4. Its definition is related to the Medial Axis of $\mathcal{M}$:

***Definition** 3.3 (Medial Axis):* A ball B is called a medial ball of $\mathcal{M}$, if B does not contain any point of $\mathcal{M}$ in its interior but at least two points of $\mathcal{M}$ on its boundary. The medial axis of $\mathcal{M}$ is the closure of the set of all midpoints of the medial balls.

Please note that the definition of medial axis in this work is similar to that in Amenta *et al*'s work [36] and Belkin *et al*'s work [1], but different from that in Plum's work [37] and Wolter's work [38].

***Definition** 3.4 (Local Feature Size):* The local feature size is the function $\rho : \mathcal{M} \to \mathbb{R}$ that assigns to $x \in \mathcal{M}$ its distance to the medial axis.

In this paper the local feature size $\rho(p)$ of a specific point p is referred as ρ to simplify the notation.

3.3 Computing the Approximation of $\Delta_{\mathcal{M}} f(p)$

To build a discrete LBO approximating the LBO $\Delta_{\mathcal{M}}$ on the point-sampled surfaces, it is necessary to approximate $\Delta_{\mathcal{M}} f(p)$ one by one for all points $p \in P$. Following is the algorithm to approximate $\Delta_{\mathcal{M}} f(p)$:

1) Tangent Plane Estimation: Set $r = 10\varepsilon$ [1], where the point cloud P is ε-sampled. Here 10ε is used to ensure that the estimated tangent plane is converging to the real tangent plane, which is proved in Belkin *et al*'s paper [1]. Consider the point set $P_r \subseteq P$ within distance r away from p, i.e., $P_r = P \cap B(p, r)$ where $B(p, r)$ is the ball centered at p with radius r. Let Q^* be the best fitting plane passing through p such that $d(P_r, Q^*)$ is minimized. Using Har-Peled and Varadarajan's algorithm [39] (also used by Belkin *et al* [1]), we construct a 2-approximation $\hat{T}_p$ of Q^*, i.e., $\hat{T}_p$ is a plane passing through p, and $d_H(P_r, \hat{T}_p) \leq 2 d_H(P_r, Q^*)$, where $d_H(\cdot, \cdot)$ is the Hausdorff distance.
2) Voronoi Cell Estimation: Fix a positive constant $\delta \geq 10\varepsilon$, and consider the set of points P_δ that are within δ away from p, i.e., $P_\delta = P \cap B(p, \delta)$. Here $\delta \geq 10\varepsilon$ is to ensure we have enough local neighboring points for approximation. We project the points in P_δ to $\hat{T}_p$. When δ is sufficiently small, this projection is bijective. We denote the projection as $\hat{\Pi}$. Then we build the Voronoi Diagram of $\hat{\Pi}(P_\delta)$ on $\hat{T}_p$. Take the area of the Voronoi cell $Vr_{\hat{T}_p}(p)$ on $\hat{T}_p$ as an approximation of the Voronoi cell area of p on surface, $Vr_{\mathcal{M}}(p)$. $Vr_{\hat{T}_p}(p)$ is also denoted as $Vr_{\hat{T}}(p)$ in this paper to simplify the notation. When the point cloud P gets denser, the area of $Vr_{\hat{T}}(p)$ is converging to the area of $Vr_{\mathcal{M}}(p)$ (Theorem 4.1).
3) Integration Approximation: We compute $\hat{\Delta}_P^t f(p)$ as an approximation to $\Delta_{\mathcal{M}} f(p)$ as follows:

$$\hat{\Delta}_P^t f(p) = \frac{1}{4\pi t^2} \sum_{q \in P_\delta} (e^{-\frac{\|q-p\|^2}{4t}} (f(q) - f(p)) \operatorname{vol}(Vr_{\hat{T}}(q))). \tag{3.3}$$

Here $\operatorname{vol}(\cdot)$ denotes the area of the given Voronoi cell. $Vr_{\hat{T}}(q)$ is the Voronoi cell of point q in its own estimated tangent plane $\hat{T}_q$. Because the new operator is defined on the point cloud P and employs the parameter t, here we denote it as $\hat{\Delta}_P^t$. The hat sign $\hat{}$ is used to differentiate it with respect to Belkin *et al*'s Δ_P^t as explained in section 3.5. $t(\varepsilon) = \varepsilon^{\frac{1}{2+\xi}}$, and $\xi > 0$ is an arbitrary selected positive fixed number, used to ensure the convergence of $\hat{\Delta}_P^t$. We are employing the Gaussian kernel to approximate the heat function locally on the manifold $\mathcal{M}$, and t is the "time" of the heat diffusion process. As the points get denser, $\hat{\Delta}_P^t$ will converge to $\Delta_{\mathcal{M}}$ (Theorem 4.2). In the following section 3.4, we assemble $\hat{\Delta}_P^t$ into its matrix form $\hat{L}_P^t$.

3.4 Discretization of the LBO

For LBO, since $< f, \Delta_{\mathcal{M}} g > = < \Delta_{\mathcal{M}} f, g >$ holds, $\Delta_{\mathcal{M}}$ is symmetric. In the discrete case, inner product is defined as $< \mathbf{f}, \mathbf{g} > = \mathbf{f}^T B \mathbf{g}$ where B is a symmetric positive-definite real matrix. Correspondingly we expect $< \mathbf{f}, L\mathbf{g} > = < L\mathbf{f}, \mathbf{g} > = \mathbf{f}BL\mathbf{g} = \mathbf{f}L^T B\mathbf{g}$ holds, where L is any discrete LBO in its matrix form. That is, $BL = L^T B = (BL)^T$ is expected to be symmetric matrix. Denote $BL = L^T B = Q$, we have $L = B^{-1}Q$ which means that the discrete LBO matrix L should be symmetrizable (self-adjoint with respect to inner product).

Belkin *et al* claimed that their discrete LBO matrix L_P^t [1] is converging point-wisely. However, their L_P^t is not guaranteed to be symmetrizable. In our application, to build the orthogonal Manifold Harmonic Bases, it is necessary to have a symmetrizable discrete Laplacian operator. A trivial way is to use

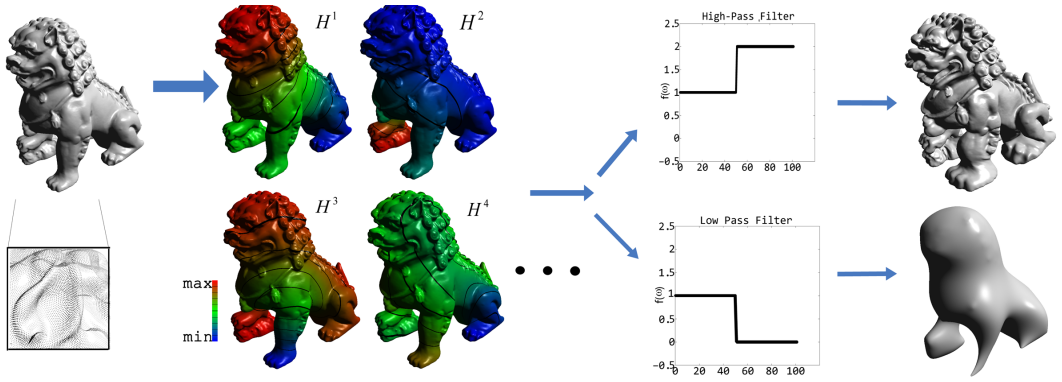

Fig. 1. From left to right: the point-sampled Chinese Lion, H^1 to H^4 bases, and two filtering results.

$(L_P^t + (L_P^t)^T)/2$ instead of L_P^t. However, our experiments in section 5 show that this trivial extension does not converge at all.

In our method, we build the discrete LBO $\hat{\Delta}_P^t$ from the equation (3.3) which is linear on the function values $f(p_i)$, for $p_i \in P$. Thus it can be written as $\hat{\Delta}_P^t f(p_i) = \hat{R}_i^T \mathbf{f}$, where $\hat{R}_i$ is an N-vector, $\mathbf{f} = [f(p_1), f(p_2), \ldots, f(p_N)]^T$ is the N-vector representing the input continuous function f sampled at the points, and $N = |P|$. Thus we have the matrix form $\hat{L}_P^t$ of our discrete LBO $\hat{\Delta}_P^t$ over the point cloud:

$$\hat{\Delta}_P^t f = \hat{L}_P^t \cdot \mathbf{f}, \tag{3.4}$$

where $\hat{R}_i^T$ is the i-th row of matrix $\hat{L}_P^t$. We can rewrite the matrix form as $\hat{L}_P^t = B^{-1} \cdot Q$, where the elements q_{ij} of the symmetric matrix Q, and the diagonal elements b_{ii} of the diagonal matrix B can be computed as follows:

$$q_{ij} = \mathrm{vol}(Vr_{\hat{T}}(p_i))\,\mathrm{vol}(Vr_{\hat{T}}(p_j))\frac{1}{4\pi t^2} e^{-\frac{\|p_i - p_j\|^2}{4t}}, \tag{3.5}$$
$$\text{where } i \neq j, \quad \|p_i - p_j\| \leq \delta,$$
$$\text{and } t(\varepsilon) = \varepsilon^{\frac{1}{2+\xi}}, \quad \xi > 0,$$
$$q_{ii} = -\sum_{j \neq i} q_{ij}, \tag{3.6}$$
$$b_{ii} = \mathrm{vol}(Vr_{\hat{T}}(p_i)). \tag{3.7}$$

By redefining the functional inner product in matrix form as $< \mathbf{f}, \mathbf{g} >= \mathbf{f}^T B \mathbf{g}$, we have:

$$\begin{aligned} < \mathbf{f}, \hat{L}_P^t \mathbf{g} > &= \mathbf{f}^T B (B^{-1} Q \mathbf{g}) \\ &= \mathbf{f}^T Q \mathbf{g} \\ &= \mathbf{f}^T Q^T (B B^{-1})^T \mathbf{g} \\ &= (B^{-1} Q \mathbf{f})^T B \mathbf{g} \\ &=< \hat{L}_P^t \mathbf{f}, \mathbf{g} >, \end{aligned}$$

which means we have the symmetrizable matrix operator $\hat{L}_P^t$ now.

3.5 Comparison with Belkin's discrete LBO L_P^t

In Belkin *et al*'s method [1], the tangent plane $\hat{T}_p$ for a specific point p is constructed with the identical

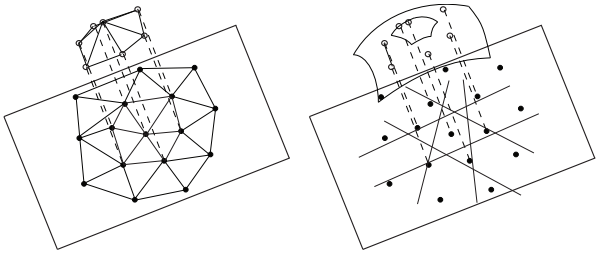

(a) (b)

Fig. 2. (a) Belkin *et al*'s approach: integration with area of triangles on the estimated tangent plane in L_P^t; (b) our approach: integration over the manifold with Voronoi cell computation on the estimated tangent plane in $\hat{L}_P^t$.

algorithm. Then $\Delta_{\mathcal{M}} f(p)$ is approximated as follows.

Fix a constant δ. Consider the set of points P_δ that are within δ away from p, i.e., $P_\delta = P \cap B(p, \delta)$. Build the Delaunay triangulation K_δ of $\hat{\Pi}(P_\delta)$ on $\hat{T}_p$. Let $K_{\frac{\delta}{2}}$ be the sub-mesh of K_δ containing triangles whose vertices are within $\frac{\delta}{2}$ away from p. Then $L_P^t f(p)$ is computed as:

$$\Delta_P^t f(p) = \frac{1}{4\pi t^2} \sum_{\sigma \in K_{\frac{\delta}{2}}} \frac{\mathrm{vol}(\sigma)}{3} \sum_{q \in V(\sigma)} (e^{-\frac{\|p - \hat{\Phi}(q)\|^2}{4t}} (f(\hat{\Phi}(q)) - f(p))), \tag{3.8}$$

where σ is a triangle in $K_{\frac{\delta}{2}}$, $V(\sigma)$ is the set of vertices of σ and $\hat{\Phi} = \hat{\Pi}^{-1}$. Then $\hat{L}_P^t$ is constructed from Δ_P^t using the similar way as introduced in section 3.4.

As mentioned earlier, to get orthogonal basis the symmetrizable discrete LBO L needs to be decomposed as $L = B^{-1}Q$ where B is real, symmetric and positive-definite and Q is symmetric and real. Here B has to be symmetric and positive-definite because it is used to define inner product. Suppose L_P^t is symmetrizable and could also be decomposed as $L_P^t = B^{-1}Q$. It is easy to see that all eigen-values of L_P^t should be real. But L_P^t does not provide real eigen-values all the time in our experiment while $\hat{L}_P^t$ does.

So we believe it is impossible to decompose L_P^t as $L_P^t = B^{-1}Q$. In other words, L_P^t is not symmetrizable.

As shown in Fig. 2, it is obvious that the difference w.r.t. our $\hat{\Delta}_P^t$ and $\hat{L}_P^t$ is: in L_P^t, the weight for point q depends on each specific point p, while in our $\hat{L}_P^t$ each point is assigned a fixed weight based on its Voronoi cell area. That is in L_P^t, the action from a certain point p to another point q is not necessarily equal to the opposite reaction from q to p. In other words, the interactions between points are not necessarily "symmetric". But in our $\hat{L}_P^t$, the interactions are always symmetric just like in LBO. We believe this is why L_P^t is not guaranteed to be symmetrizable while $\hat{L}_P^t$ is. So L_P^t can not be used for computing orthogonal Manifold Harmonics while our $\hat{L}_P^t$ can.

3.6 Point-Based Manifold Harmonic Transform

Having the symmetrizable LBO matrix operator $\hat{L}_P^t = B^{-1} \cdot Q$, we can solve the following generalized eigen problem:

$$QH = -\lambda BH. \tag{3.9}$$

By solving this problem, we have eigen-values $\{\lambda_i\}$ and corresponding eigen-vectors $\{H^i\}$. $\{H^i\}$ are called the *Point-Based Manifold Harmonic Bases* (PB-MHB) of the sampled manifold surface. PB-MHB can be used for the general spectral processing of 3D models.

Without any loss of generality, we assume that all the eigen-vectors are normalized $< H^i, H^i >= (H^i)^T B H^i = 1$, and $\lambda_i \leq \lambda_j$ holds for all $i < j$. Because $< H^i, H^j >= (H^i)^T B H^i = \delta_{ij}$ holds where δ_{ij} is Kronecker delta, the eigen-vectors $\{H^i\}$ can be used in Fourier-like spectral decomposition for functions defined over point-sampled manifold surfaces:

$$\tilde{f}_i =< \mathbf{f}, H^i >= \mathbf{f}^T B H^i, \tag{3.10}$$

where $\mathbf{f}$ is the vector of function values sampled on the point cloud. This process is called *Point-Based Manifold Harmonic Transform* (PB-MHT). With $\{\tilde{f}_i\}$, we can reconstruct $\mathbf{f}$ using the Inverse PB-MHT:

$$\mathbf{f} = \sum \tilde{f}_i \cdot H^i \tag{3.11}$$

We can consider the coordinates of the points as three continuous functions defined over the manifold surface: $\mathbf{x}$, $\mathbf{y}$ and $\mathbf{z}$. By employing PB-MHT presented above, we can decompose the manifold surface into its spectral representation $(\tilde{x}_i, \tilde{y}_i, \tilde{z}_i)$ and recover them using the Inverse PB-MHT. In section 5 we show the results of applying some spectral filters on general point-sampled surfaces, by modifying their spectral representations $\{(\tilde{x}_i, \tilde{y}_i, \tilde{z}_i)\}$. Figure 1 shows the results of applying two spectral filters on the point-sampled Chinese Lion model. This can be used to remove noises from scanned surfaces or to enhance detailed features.

4 Convergence Theorems

In Belkin *et al*'s work [1], the convergence of discrete LBO L means $L\mathbf{f}$ is converging to $\Delta_{\mathcal{M}} f$ point-wisely where $\mathbf{f}$ is the discrete form of function f. In works related to finite element method, this property is called consistency of operator [9] while convergence of operator has different definition [25]. In this work we take the definition in Belkin *et al*'s work.

In our construction of PB-MHB, the assumption is we have a continuous closed differentiable Riemannian manifold $\mathcal{M}$ on which the sample set P lies. f is a C^2 continuous function defined over $\mathcal{M}$. To show that this method is geometry-aware, we are going to prove that the result of our discrete LBO applied on the function $\hat{L}_P^t\mathbf{f}$ converges to the continuous result $\Delta_{\mathcal{M}} f$ point-wisely.

To show the convergence of $\hat{L}_P^t$, first in Theorem 4.1 we show that our estimation of the Voronoi cell area is converging to the real Voronoi cell area as point clouds get denser. With the Voronoi cell area convergence result, in Theorem 4.2 we show that $\hat{L}_P^t\mathbf{f}$ converges to $\Delta_{\mathcal{M}} f$ point-wisely. The proofs are provided in the supplementary appendices.

***Theorem** 4.1 (Voronoi Cell Approximation):* Consider the Voronoi cell of point $p \in P$ where P is a $(\varepsilon, s\varepsilon)$-sample of the manifold $Vr_{\mathcal{M}}(p)$, and the Voronoi cell on its estimated tangent plane $Vr_{\hat{T}}(p)$ built with our algorithm,

$$\left\| \frac{\text{vol}(Vr_{\mathcal{M}}(p))}{\text{vol}(Vr_{\hat{T}}(p))} - 1 \right\| \leq O(\varepsilon^2/\rho^2) \tag{4.1}$$

holds when ε is small enough.

***Theorem** 4.2 (Convergence of $\hat{\Delta}_P^t$ to $\Delta_{\mathcal{M}}$):* Consider an $(\varepsilon, s\varepsilon)$-sample P of the closed manifold surface $\mathcal{M}$, and an arbitrary function $f \in C^2$, our discrete LBO operator $\hat{\Delta}_P^t$ satisfies:

$$\lim_{\varepsilon \to 0} \|\hat{\Delta}_P^t f - \Delta_{\mathcal{M}} f\|_\infty = 0, \tag{4.2}$$

where $t(\varepsilon) = \varepsilon^{\frac{1}{2+\xi}}$, and $\xi > 0$ is any positive fixed number.

5 Experimental Results

Experiments were conducted to verify the convergence property of our operator $\hat{L}_P^t$ addressed in section 4, the convergence property of the eigen-vectors $\{H^i\}$, the geometry-awareness of $\{H^i\}$, and applications of PB-MHT. In our implementation, the generation of LBO matrix is developed using MinGW, the eigen problem is solved in MATLAB, and the filtering and rendering parts are written in Visual C++. We conducted experiments on a Windows XP platform with Intel Core 2 Duo 2.66GHz CPU and 2GB DDR2 RAM. Table 1 shows the model information and the running time of our experiments.

TABLE 1
Model information and running time (in seconds) for computing LBO matrix (t_{LBO}) and solving the eigen-vectors (t_{eigen}).

Model	#Points	t_{LBO}	#Bases	t_{eigen}
Sphere	4,002	156	100	2.8
Eight	7,678	401	100	17
Cylinder	90,300	6,426	100	348
Rabbit	248,304	12,198	100	2,051
Chinese Lion	611,222	25,214	100	7,269

5.1 Convergence of Laplace-Beltrami Operator

To verify the convergence of our discrete LBO matrix $\hat{L}_P^t$, we used a cylinder model with radius 1, height 4, and 90,300 vertices. We parameterized this cylinder surface as:

$$x = \cos\alpha, \tag{5.1}$$
$$y = \sin\alpha, \tag{5.2}$$
$$z = v, \tag{5.3}$$

where α and v are the parameters: $0 \le \alpha < 2\pi$, $0 < v < 4$. We sampled the cylinder circle with 300 points, and sampled the v direction with 301 points. We defined the function f over the cylinder surface as:

$$f(p) = v^2. \tag{5.4}$$

The analytical solution of the LBO applied on the function f is $\Delta_{\mathcal{M}} f = 2$, for $v > 0$ over this cylinder surface. In this paper we only consider closed surfaces, but it is impractical to conduct experiments on infinite-length cylinder surfaces. So in our experiments we used the cylinder model of finite length and ignored the solutions for points near the boundary to verify the performance of LBO convergence on the infinite cylinder surface. We gave each point an index according to its v parameter value. Figure 3 shows the approximation results of our discrete LBO applied on the function (a) $\hat{L}_P^t\mathbf{f}$, as compared to (b) Belkin *et al*'s discrete LBO $L_P^t\mathbf{f}$, (c) the graph Laplacian $L_G\mathbf{f}$, and (d) the trivial extension of $1/2 \cdot (L_P^t + (L_P^t)^T)\mathbf{f}$. If we ignore the cylinder boundary points, which indices are close to 0 and 9×10^4 as in Fig. 3, we can see that: (a) our $\hat{L}_P^t$ is converging perfectly; (b) Belkin *et al*'s L_P^t has slight oscillations; (c) the graph Laplacian L_G gives constant 0 values incorrectly; and (d) the trivial extension $(L_P^t + (L_P^t)^T)/2$ does not converge at all.

The reason why Belkin *et al*'s discrete LBO L_P^t has more error, as shown in Fig. 2(a), is that L_P^t is actually trying to compute the integration on estimated tangent planes rather than the integration over the manifold as proposed by Lemma 5 in [28]. Although this is still converging, there may be more error. In Fig. 3, the point index depends on v parameter, that is, the higher the index, the higher function value will the point and its neighbours have, since $f(p) = v^2$. This may "amplify" the error as the index gets larger. Our

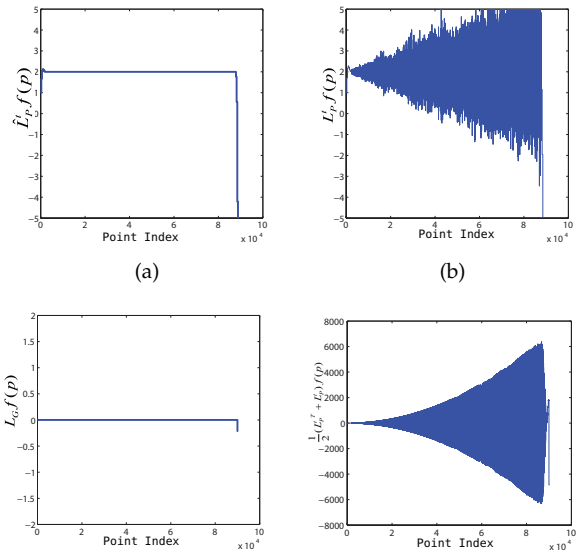

Fig. 3. LBO approximation result on the cylinder surface: (a) our Voronoi cell-based discrete LBO $\hat{L}_P^t$; (b) Belkin *et al*'s discrete LBO L_P^t; (c) the graph Laplacian operator L_G; (d) the trivial extension $(L_P^t + (L_P^t)^T)/2$. Note that (d) has much larger scale than others.

discrete LBO $\hat{L}_P^t$, as shown in Fig. 2(b), approximates the integration over the manifold directly with the estimated Voronoi cell area.

LBO on the 2-sphere in $\mathbb{R}^3$ is well studied. The eigen-functions of LBO over the sphere are called Spherical Harmonics and denoted as Y_l^m with degree l and order m. In spherical coordinates, the eigen-function of LBO with the smallest non-zero eigen-value $\lambda = 2$ on the unit sphere is $Y_1^0 = \cos\theta$. That is, $\Delta_{S(2)} Y_1^0 = -2Y_1^0$. We used three point clouds sampled from the 2-sphere of unit radius: uniform 1,000 points, uniform 3,994 points, and 2,475 points with different resolutions on its two hemispheres, as shown in Fig. 4. For each point, we computed the error between the approximated $\Delta_{S(2)} Y_1^0$ and the analytical result $-2Y_1^0$. Figure 5 shows the error histograms of $\hat{L}_P^t$ and L_P^t on these sphere models with input function $f = Y_1^0$. In all cases $\hat{L}_P^t$ has less error than L_P^t.

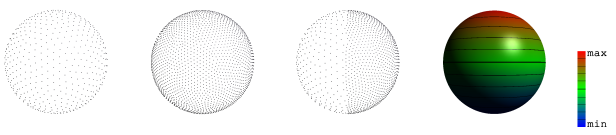

Fig. 4. Different point clouds sampled on unit sphere: (a) uniform 1,000 points; (b) uniform 3,994 points; (c) non-uniform 2,475 points; (d) Spherical Harmonics Y_1^0 on unit sphere.

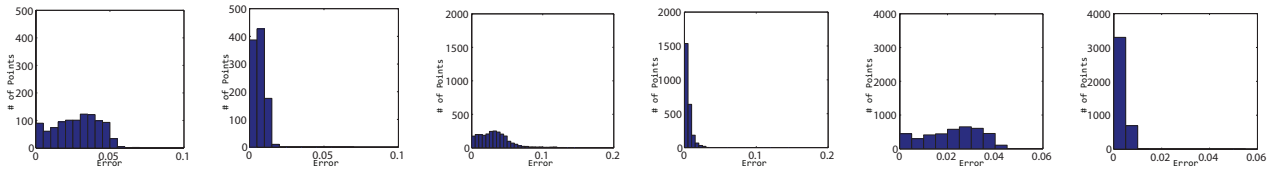

(a) (b) (c) (d) (e) (f)

Fig. 5. Approximation result of $\Delta_{S(2)} Y_1^0$ on the unit sphere. (a), (c), (e) are the error histograms of Belkin *et al*'s discrete LBO L_P^t; (b), (d), (f) are the error histograms of our discrete LBO $\hat{L}_P^t$: (a), (b) uniformly sampled 1,000 points; (c), (d) non-uniformly sampled 2,475 points; (e), (f) uniformly sampled 3,994 points.

5.2 Convergence of Manifold Harmonics

We use the same sphere models as in section 5.1. In spherical coordinates, we have $Y_1^0 = \cos\theta$ which is the spherical harmonics with the smallest non-zero eigen-value. In the spectrum of the unit 2-sphere in $\mathbb{R}^3$, Y_1^0 has multiplicity of 3 with $\lambda = 2$. In other words, Y_1^0 appears 3 times as f_{Y1}, f_{Y2} and f_{Y3} with different rotation. Note that any linear combination $f_Y = af_{Y1} + bf_{Y2} + cf_{Y3}$ is also an eigen-function with $\lambda = 2$. More specifically, f_Y is a scaled Y_1^0 that is rotated over the surface with some angle. Given one of the first 3 eigen-vectors H of any discrete LBO, we need to find such a f_Y that fits it best. Consider the square error $\mathcal{E}_2 = \sum_{p_j} (H(p_j) - f_Y(p_j))^2$ as a function of a, b and c that are real numbers, and $p_j \in P$. We take the f_Y that minimizes $\mathcal{E}_2$ as the best-fit. The minimal value is achieved when the partial derivatives of $\mathcal{E}_2$ with respect to a, b and c are 0. By solving this problem we have the best-fit f_Y. This f_Y is then used to calculate the error for the eigen-vectors.

Our PB-MHB can be directly used on point-sampled surfaces. So we compared it with the eigen-vectors of other combinatorial Laplacian operators, such as the normalized graph Laplacian (GL), Kirchhoff Laplacian (KL), and Tutte Laplacian (TL), by creating the connectivity between points using the ε-ball. Denote the degree of point p_i as d_i. Define the adjacency matrix $\mathcal{A}$ as $\mathcal{A}_{ij} = 1$ when (p_i, p_j) is an edge , and $\mathcal{A}_{ij} = 0$ otherwise. GL is defined as: $\mathcal{G} = \mathcal{I} - Q$, where $Q_{ij} = Q_{ji} = \mathcal{A}_{ij}/\sqrt{d_i d_j}$ and $\mathcal{I}$ is the identity matrix; KL matrix $\mathcal{K}$ is defined by: $\mathcal{K}_{ij} = d_i$ if $i = j$, and $\mathcal{K}_{ij} = -1$ if $i \neq j$ and (p_i, p_j) is an edge; and TL is defined as: $\mathcal{T} = \mathcal{I} - \mathcal{C}$, where $\mathcal{C}_{ij} = 1/d_i$ if and only if (p_i, p_j) is an edge. These operators were studied extensively in Zhang's work [32].

Table 2 shows the errors of the first 3 eigen-vectors with the non-zero eigen-values of $\hat{L}_P^t$, GL $\mathcal{G}$ and KL $\mathcal{K}$. TL $\mathcal{T}$ is not presented because it is not symmetrizable and has complex eigen-values and eigen-vectors. Here we use $\mathcal{E}_{inf} = \max_{p_j} (f_Y(p_j) - H(p_j))$ where $p_j \in P$, to represent the error of each eigen-vector. Because eigen-vector multiplied with a constant number is still eigen-vector, the maximum and minimum of each eigen-vector are also provided as range. We can see that eigen-values and eigen-vectors of our $\hat{L}_P^t$ are very close to the analytical result 2 and Y_1^0, respectively. Those of $\mathcal{G}$ and $\mathcal{K}$ are not.

Figure 6 shows the first three eigen-vectors of the graph Laplacian L_G, which are not close to the analytical counterpart as shown in Fig. 4(d). We can easily see the distortion of the iso-contour lines of the eigen-functions.

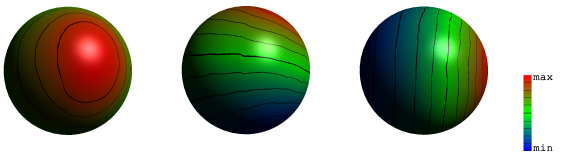

(a) (b) (c)

Fig. 6. Eigen-vectors of graph Laplacian L_G on the non-uniform sphere model as in figure 4(c): (a) H^1; (b) H^2; (c) H^3.

5.3 Non-Uniformly-Sampled Point Cloud

Our experiments show that as long as the point cloud P is $(\varepsilon, s\varepsilon)$-sampled, and the local feature sizes ρ are not close to zero (since our discrete LBO convergence rate is $O(\frac{\varepsilon^2}{\rho^2})$), our PB-MHB is geometry-aware and independent of the sampling rate. We conducted our experiment on the "symmetric" two-hole torus ("Eight") model, where the point sampling rate over the two handles are different. As shown in Fig. 7, when the point distribution is non-uniform, the first 4 bases of our PB-MHB are still symmetric over the surface, while the eigen-vectors of the graph Laplacian operator can not follow the geometric property of the surface.

5.4 Spectral Filtering

Spectral filtering could be used for model manipulation such as noise-removing. Having the PB-MHB, we can apply filtering on the spectral representation of point-sampled surfaces. As shown in Fig. 1, we can apply either "low-pass filtering" or "detail-enhancement" on the point-sampled Chinese Lion model. Note that even when points are non-uniformly distributed, as shown in Fig. 8 where the left-part of the Rabbit model is sparser than the right-part,

TABLE 2
Approximation results of eigen-vectors of $\hat{L}_P^t$, $\mathcal{G}$ and $\mathcal{K}$ defined on unit spheres.

#Points	H	PB-MHB			GL $\mathcal{G}$			KL $\mathcal{K}$		
		Range	$\mathcal{E}_{\text{inf}}$	λ	Range	$\mathcal{E}_{\text{inf}}$	λ	Range	$\mathcal{E}_{\text{inf}}$	λ
$1,000$	H^1	$[-0.5, 0.5]$	0.0006	1.9882	$[-0.05, 0.05]$	0.0017	0.1512	$[-0.05, 0.05]$	0.0026	24.13
	H^2		0.0004	1.9890	$[-0.05, 0.05]$	0.0026	0.1567	$[-0.06, 0.05]$	0.0029	24.75
	H^3		0.0004	1.9903	$[-0.05, 0.05]$	0.0022	0.1658	$[-0.06, 0.06]$	0.0028	25.84
Non-Uniform $2,475$	H^1		0.0058	1.9779	$[-0.03, 0.04]$	0.014	0.0567	$[-0.01, 0.08]$	0.058	4.556
	H^2		0.0007	1.9913	$[-0.04, 0.04]$	0.015	0.0598	$[-0.06, 0.06]$	0.044	8.618
	H^3		0.0013	1.9917	$[-0.01, 0.08]$	0.057	0.0696	$[-0.06, 0.06]$	0.044	8.718
$3,994$	H^1		0.0003	1.9952	$[-0.03, 0.03]$	0.0013	0.0376	$[-0.03, 0.03]$	0.0014	6.04
	H^2		0.0003	1.9953	$[-0.03, 0.03]$	0.0015	0.0391	$[-0.03, 0.03]$	0.0015	6.199
	H^3		0.0003	1.9957	$[-0.03, 0.03]$	0.0014	0.0421	$[-0.03, 0.03]$	0.0013	6.525

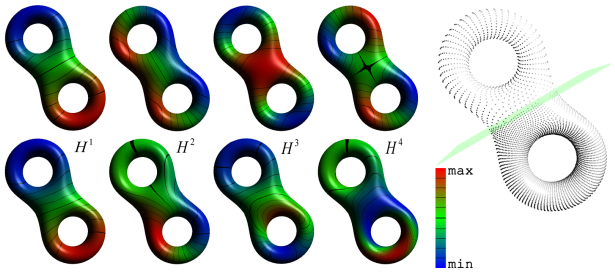

Fig. 7. The eigen-functions H^1, H^2, H^3, and H^4 of our $\hat{L}_P^t$ (first row) and the graph Laplacian operator L_G (second row), for the symmetric model "Eight" with non-uniform sampling rate.

our PB-MHT can still get "symmetric" filtering result, while the graph Laplacian method makes the left-part "shrink" more than the right-part. Figure 9 shows the example of removing the high-frequency noises on the sphere by applying the low-pass filter with PB-MHT, which still preserves the symmetry of the sphere.

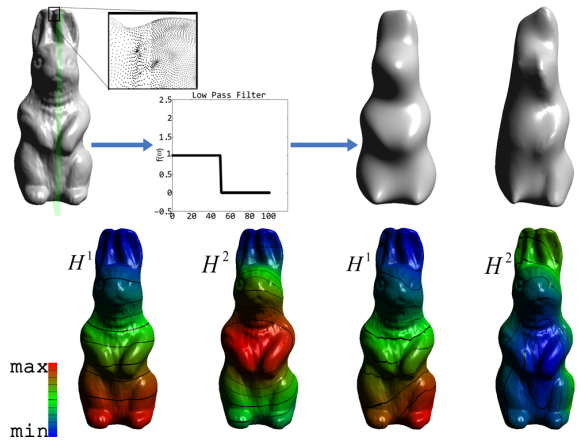

Fig. 8. First row: the Rabbit model with non-uniform sampling, and the low-pass filtered model: using our $\hat{L}_P^t$ (left) and graph Laplacian operator L_G (right). Second row: H^1 and H^2 of our $\hat{L}_P^t$ (left) and the graph Laplacian operator L_G (right). It is obvious that $\hat{L}_P^t$ is geometry-aware and L_G is not.

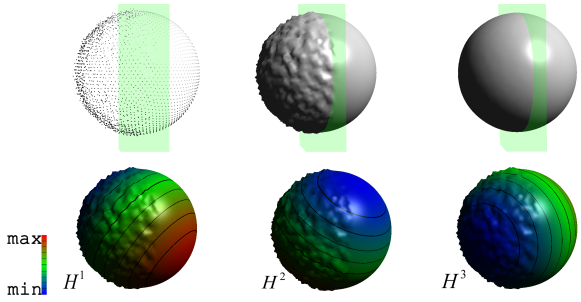

Fig. 9. First row: the sphere model with noises on its left side, before and after the low-pass filtering. Second row: the H^1, H^2, and H^3 bases.

5.5 Salient Feature Point Extraction

MHB on mesh surface is used to extract salient feature points by Hu *et al* [40]. With eigen-vectors $\{H^i\}$ of the discrete LBO, a point p is selected as salient feature point if $H^i(p)$ is larger than its neighboring points in both of the adjacent two frequencies H^i and H^{i+1}. Note that such feature point extraction algorithm requires MHB to be fully geometry-aware and independent of the sampling rate and mesh connectivity.

For point-sampled surfaces, our PB-MHB can be directly used to extract salient feature points using this algorithm. We compared the performance with the eigen-vectors of normalized graph Laplacian (GL), Kirchhoff Laplacian (KL), and Tutte Laplacian (TL), by creating the connectivity between points using the ε-ball. Because TL $\mathcal{T}$ has complex eigen-vectors which is not applicable, we used the real part of the eigen-vectors instead.

As shown in Fig. 10 and 11, PB-MHB could provide very stable feature points despite the different resolutions of the input models, while the other combinatorial Laplacian operators could not.

5.6 Discussion: Performance Degradation Near Open Boundaries and Sharp Edges

When there are open boundaries or sharp edges, the procedure described in section 3 may encounter problems. In these cases the Voronoi Cell Estimation process described in section 3.3 may get either

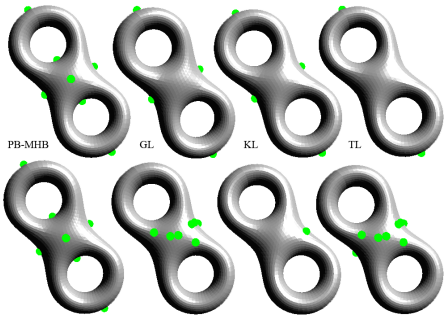

Fig. 10. Extracting feature points from the two-hole torus model using our PB-MHB, and the eigen-vectors of GL, KL, and TL methods, with (first row) regular resolution, and (second row) irregular resolution as in Fig. 7.

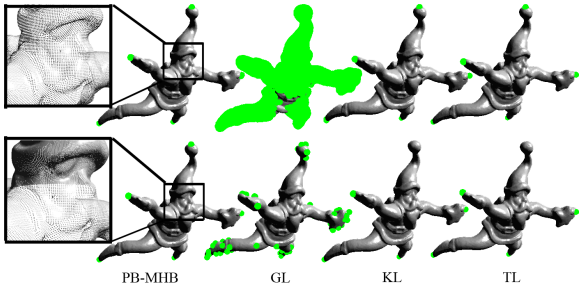

Fig. 11. Extracting feature points from the Santa model using our PB-MHB, and the eigen-vectors of GL, KL, and TL methods, with (first row) regular resolution of $75,781$ vertices, and (second row) irregular resolution of $122,292$ vertices.

open or very slim Voronoi cells on the estimated tangent plane, and may not provide valid cell areas. These points are referred as *invalid points*. Our current method is based on the assumption that the point cloud is $(\varepsilon, s\varepsilon)$-sampled, and the local feature sizes ρ are not close to zero. When there are sharp edges, the local feature sizes at those sharp edges tend to be zero. Since our convergence rate of the estimated Voronoi cell area is $O(\frac{\varepsilon^2}{\rho^2})$, if the point cloud is not dense enough locally at those regions, this algorithm will have difficulty in converging to the continuous counterpart.

We conducted the following experiments to explore such performance degradation. Since the Voronoi cells of the invalid points are either open or slim (degenerate), we took the average Voronoi cell area of the valid points as the Voronoi cell areas of those invalid points. Although such slight modification makes this method applicable for models with open boundaries and sharp edges, the convergence of both LBO and MHB gets degraded. To verify the convergence degradation, we performed experiments on a unit flat square model with an open boundary. The model was sampled with 101 points in both u and v direction where u and v are the parametric coordinates. To create sharp ridge, we folded the model along the line of $v = 0.5$ by different angles as shown in Fig. 12. Because the folding process is isometric, $\Delta_{\mathcal{M}}$ remains the same no matter how much we fold the model.

As shown in Fig. 12, the symmetry of MHB on the flat square model is well preserved. However, the MHB varies as the ridge gets sharper.

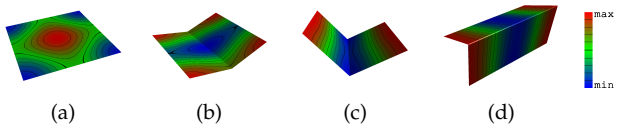

Fig. 12. H^4 of (a) flat square model sampled with 101x101 points; and the same model folded by (b) 30 degree, (c) 70 degree, and (d) 120 degree.

To further demonstrate the effect of different sharp ridges on $\hat{L}_P^t$, we defined a scalar function $f = v$ and applied $\hat{L}_P^t$ on it. The analytical result is $\Delta_{\mathcal{M}} f = 0$ no matter how we fold the square model. As shown in Fig. 13, on flat square model the error of $\hat{L}_P^t f$ is very little except for the boundary points. When we fold the model as shown in Fig. 12, the error increases for points near the ridge (middle part of the graph). The sharper the ridge is, the higher error we get. Note that the boundary points along u direction have very large error while the others along v do not, as shown in Fig. 13. This is due to the reason that we used the function $f = v$, and $\Delta_{\mathcal{M}} f(p)$ is approximated by the local integration near the point p. Because boundary points miss part of their neighbors, the integration could be approximated only on part of the domain for them. When the integration result for the missing part is close to 0 the error will be negligible (along v direction), otherwise the error could be very large (along u direction).

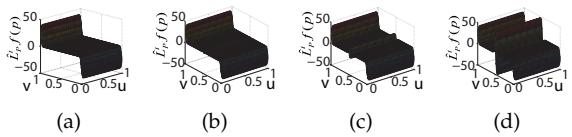

Fig. 13. $\hat{L}_P^t f$ for function $f = v$ on (a) flat square model sampled with 101x101 points; and the same model folded by (b) 30 degree, (c) 70 degree, and (d) 120 degree.

6 Conclusion and Future Work

The mesh-based Manifold Harmonics [4], [5] provides spectral processing framework for 3D models. However, it can not be applied to point clouds directly. In this paper, we propose a new method to compute the *symmetrizable* and *converging* discrete LBO matrix $\hat{L}_P^t$ on the manifold surface $\mathcal{M}$ represented by the point cloud P. We prove that $\hat{L}_P^t$ is converging point-wisely to the LBO $\Delta_{\mathcal{M}}$ given that P is $(\varepsilon, s\varepsilon)$-sampled, and

the local feature sizes ρ at the points are not close to zero. With the symmetrizable property of $\hat{L}_P^t$, we can compute the Point-Based Manifold Harmonic Bases $\{H^i\}$ on point clouds by solving the eigen problem $\hat{L}_P^t f = -\lambda f$. The orthogonal bases can be used to perform spectral transformation and processing directly on point clouds without computing the explicit global mesh. Our experiments show that $\hat{L}_P^t$ is fully geometry-aware, and converges very well as compared to other discrete combinatorial Laplacian operators, such as the graph Laplacian, Kirchhoff Laplacian, Tutte Laplacian, and the trivial extension of Belkin *et al*'s discrete operator [1]. We also demonstrate that our PB-MHT can be used as an effective spectral analysis and processing tool for point-sampled manifold surfaces.

There are also some limitations about our current approach, which motivates our future researches along this direction of point-based spectral processing. First of all, this method is designed for closed manifold surfaces. When there is boundary on surfaces, it is hard for the algorithm to estimate the Voronoi cell area near the boundary, since the cell is open. Thus the convergence of this method degrades significantly at the boundary points. We will investigate robust algorithms for open point-sampled surfaces. Second, for the surface regions with high curvature, our current method requires high sampling rates to produce meaningful discrete operator. When there are sharp edges or spikes in the model, the convergence will degrade because the local feature sizes at those sharp edges or spikes tend to be zero. Computing LBO and MHB for the point-sampled surfaces with sharp features will be an interesting research avenue for the future.

ACKNOWLEDGEMENTS

We would like to thank the anonymous reviewers for their constructive comments and Dr. Jian Sun for the source code and helpful advices. This research is partially supported by the National Science Foundation under Grants No. CNS-1012975 and CCF-0727098.

REFERENCES

[1] M. Belkin, J. Sun, and Y. Wang, "Constructing Laplace operator from point clouds in $\mathbb{R}^d$," in *Proceedings of the 19th Annual ACM-SIAM Symposium on Discrete Algorithms*. Philadelphia, PA, USA: Society for Industrial and Applied Mathematics, 2009, pp. 1031–1040.

[2] S. Rosenberg, *The Laplacian on a Riemannian Manifold: An Introduction to Analysis on Manifolds*, ser. London Mathematical Society Student Texts. Cambridge University Press, 1997.

[3] J. Jost, *Riemannian Geometry and Geometric Analysis*, ser. Universitext. Berlin New York: Springer, 2002.

[4] M. Reuter, F.-E. Wolter, and N. Peinecke, "Laplace-Beltrami spectra as "shape-DNA" of surfaces and solids," *Computer-Aided Design*, vol. 38, no. 4, pp. 342–366, 2006.

[5] B. Vallet and B. Lévy, "Spectral geometry processing with manifold harmonics," *Computer Graphics Forum*, vol. 27, no. 2, pp. 251–260, 2008.

[6] J. Hu and J. Hua, "Salient spectral geometric features for shape matching and retrieval," *The Visual Computer*, vol. 25, no. 5-7, pp. 667–675, 2009.

[7] H. Zhang, O. van Kaick, and R. Dyer, "Spectral methods for mesh processing and analysis," in *Proceedings of Eurographics State-of-the-art Report*, 2007, pp. 1–22.

[8] N. Peinecke, F.-E. Wolter, and M. Reuter, "Laplace spectra as fingerprints for image recognition," *Computer Aided Design*, vol. 39, pp. 460–476, June 2007. [Online]. Available: http://portal.acm.org/citation.cfm?id=1244485.1244880

[9] K. Hildebrandt and K. Polthier, "On approximation of the laplace-beltrami operator and the willmore energy of surfaces," *Computer Graphics Forum*, pp. 1513–1520, 2011.

[10] K. Huseyin, *Vibration and Stability of Multiple Parameter Systems*. Springer.

[11] B. Lévy, "Laplace-Beltrami eigenfunctions towards an algorithm that "understands" geometry," *Shape Modeling and Applications, International Conference on*, vol. 0, p. 13, 2006.

[12] L. Miao, J. Huang, X. Liu, H. Bao, Q. Peng, and B. Guo, "Computing variation modes for point set surfaces," in *Point-Based Graphics, 2005. Eurographics/IEEE VGTC Symposium Proceedings*, June 2005, pp. 63–69.

[13] G. Taubin, "A signal processing approach to fair surface design," in *Proceedings of SIGGRAPH'95*. New York, NY, USA: ACM, 1995, pp. 351–358.

[14] R. Liu and H. Zhang, "Mesh segmentation via spectral embedding and contour analysis," *Computer Graphics Forum*, vol. 26, pp. 385–394, 2007.

[15] Z. Karni and C. Gotsman, "Spectral compression of mesh geometry," in *Proceedings of SIGGRAPH'00*, 2000, pp. 279–286.

[16] D. Cotting, T. Weyrich, M. Pauly, and M. Gross, "Robust watermarking of point-sampled geometry," in *Proceedings of the Shape Modeling International*, 2004, pp. 233–242.

[17] J. Wu and L. Kobbelt, "Efficient spectral watermarking of large meshes with orthogonal basis functions," *The Visual Computer*, vol. 21, no. 8–10, pp. 848–857, 2005.

[18] S. Dong, P.-T. Bremer, M. Garland, V. Pascucci, and J. C. Hart, "Spectral surface quadrangulation," *ACM Transactions on Graphics*, vol. 25, no. 3, pp. 1057–1066, 2006.

[19] J. Huang, M. Zhang, J. Ma, X. Liu, L. Kobbelt, and H. Bao, "Spectral quadrangulation with orientation and alignment control," *ACM Transactions on Graphics*, vol. 27, no. 5, p. 147, 2008.

[20] P. Mullen, Y. Tong, P. Alliez, and M. Desbrun, "Spectral Conformal Parameterization," *Computer Graphics Forum*, vol. 27, pp. 1487–1494, 2008.

[21] M. Desbrun, M. Meyer, P. Schröder, and A. H. Barr, "Implicit fairing of irregular meshes using diffusion and curvature flow," in *Proceedings of SIGGRAPH'99*. New York, NY, USA: ACM Press/Addison-Wesley Publishing Co., 1999, pp. 317–324.

[22] M. Meyer, M. Desbrun, P. Schröder, and A. Barr, "Discrete differential-geometry operator for triangulated 2-manifolds," in *Proceedings of Visual Mathematics'02*, 2002.

[23] G. Xu, "Discrete Laplace-Beltrami operators and their convergence," *Computer Aided Geometric Design*, vol. 21, no. 8, pp. 767–784, 2004.

[24] U. Pinkall and K. Polthier, "Computing discrete minimal surfaces and their conjugates," *Experimental Mathematics*, vol. 2, no. 1, pp. 15–36, 1993.

[25] K. Hildebrandt, K. Polthier, and M. Wardetzky, "On the convergence of metric and geometric properties of polyhedral surfaces," *Geometriae Dedicata*, vol. 123, no. 1, pp. 89–112, 2006.

[26] M. Wardetzky, S. Mathur, F. Kälberer, and E. Grinspun, "Discrete laplace operators: no free lunch," in *Proceedings of the 5th Eurographics Symposium on Geometry Processing*. Aire-la-Ville, Switzerland, Switzerland: Eurographics Association, 2007, pp. 33–37.

[27] M. Reuter, S. Biasotti, D. Giorgi, G. Patan, and M. Spagnuolo, "Discrete laplace-beltrami operators for shape analysis and segmentation," *Computers & Graphics*, vol. 33, no. 3, pp. 381 – 390, 2009, IEEE International Conference on Shape Modelling and Applications 2009.

[28] M. Belkin and P. Niyogi, "Towards a theoretical foundation for Laplacian-based manifold methods," in *Lecture Notes on Computer Science*. Springer-Verlag, 2005, vol. 3559/2005, pp. 486–500.

[29] M. Belkin, J. Sun, and Y. Wang, "Discrete Laplace operator on meshed surfaces," in *Proceedings of the 24th Annual Symposium on Computational Geometry*. New York, NY, USA: ACM, 2008, pp. 278–287.
[30] T. K. Dey, P. Ranjan, and Y. Wang, "Convergence, stability, and discrete approximation of laplace spectra," in *Proceedings of the ACM-SIAM Symposium on Discrete Algorithms*, 2010, pp. 650–663.
[31] R. R. Coifman and S. Lafon, "Diffusion maps," *Applied and Computational Harmonic Analysis*, vol. 21, no. 1, pp. 5 – 30, 2006, Diffusion Maps and Wavelets.
[32] H. Zhang, "Discrete combinatorial laplacian operators for digital geometry processing," in *Proceedings of SIAM Conference on Geometric Design and Computing*. Nashboro Press, 2004, pp. 575–592.
[33] C. Luo, J. Sun, and Y. Wang, "Integral estimation from point cloud in d-dimensional space: a geometric view," in *SCG '09: Proceedings of the 25th annual symposium on Computational geometry*. New York, NY, USA: ACM, 2009, pp. 116–124.
[34] N. Amenta, M. Bern, and M. Kamvysselis, "A new Voronoi-based surface reconstruction algorithm," in *Proceedings of SIGGRAPH'98*. New York, NY, USA: ACM, 1998, pp. 415–421.
[35] J. Giesen and U. Wagner, "Shape dimension and intrinsic metric from samples of manifolds with high co-dimension," in *Proceedings of the 19th Annual Symposium on Computational Geometry*. New York, NY, USA: ACM, 2003, pp. 329–337.
[36] N. Amenta and M. Bern, "Surface reconstruction by Voronoi filtering," in *Proceedings of the 14th Annual Symposium on Computational Geometry*. New York, NY, USA: ACM, 1998, pp. 39–48.
[37] H. Blum, "A Transformation for Extracting New Descriptors of Shape," in *Models for the Perception of Speech and Visual Form*, W. W. Dunn, Ed. Cambridge: MIT Press, 1967, pp. 362–380.
[38] F. E. Wolter, "Cut locus & medial axis in global shape interrogation & representation," 1992.
[39] S. Har-Peled and K. Varadarajan, "Projective clustering in high dimensions using core-sets," in *Proceedings of the 18th Annual Symposium on Computational Geometry*. New York, NY, USA: ACM, 2002, pp. 312–318.
[40] J. Hu and J. Hua, "Salient spectral geometric features for shape matching and retrieval," *The Visual Computer*, vol. 25, no. 5, p. 667C675, 2009.

Yang Liu received BS degree in computer science and technology from the Tsinghua University in 2001 and the MS degree in computer software and theory from the Institute of Software, Chinese Academy of Science in 2005. He is currently a PhD candidate in computer science at University of Texas at Dallas. His research interests are in computer graphics, spectral geometric analysis and digital watermarking for multimedia content. For more information, see http://www.utdallas.edu/~yxl072100/.

Dr. Balakrishnan Prabhakaran is currently Professor of Computer Science in the University of Texas at Dallas. He received his PhD in Computer Science from Indian Institute of Technology, Madras, India in 1995. He has been working in the area of multimedia systems : animation & multimedia databases, authoring & presentation, resource management, and scalable webbased multimedia presentation servers. Dr. Prabhakaran received the prestigious National Science Foundation (NSF) CAREER Award in 2003 for his proposal on Animation Databases. He is the General co-Chair for ACM Multimedia 2011. He has served as an Associate Chair of the ACM Multimedia Conferences in 2006, 2003, 2000 and 1999. He has served as guest-editor of special issues on various topics for different multimedia journals. He is also serving on the editorial board of journals such as Multimedia Systems (Springer), Multimedia Tools and Applications (Springer), Journal of Multimedia (Academy Publishers), and Journal of Multimedia Data Engineering and Management (Information Resources Management Association (IRMA)). He is also the Editor-in-chief of the ACM SIGMM (Special Interest Group on Multimedia) Online magazine.

Xiaohu Guo received the PhD degree in computer science from the State University of New York at Stony Brook in 2006. He is an assistant professor of computer science at the University of Texas at Dallas. His research interests include computer graphics, animation and visualization, with an emphasis on geometric, and physics-based modeling. His current researches at UT-Dallas include: spectral geometric analysis, deformable models, centroidal Voronoi tessellation, GPU algorithms, 3D and 4D medical image analysis, etc. He is a member of the IEEE. For more information, please visit http://www.utdallas.edu/~xguo.

Supplemental Appendices

This document provides information about convergence of $\hat{L}_P^t$.

In Belkin *et al.*'s work [1], the convergence of $\hat{L}_P^t$, means $L\mathbf{f}$ is converging to $\Delta_{\mathcal{M}} f$ point-wisely where $\mathbf{f}$ is the discrete form of function f. This is different from the definition of convergence in works related to finite element method [2], [3]. We take the definition in Belkin *et al.*'s work [1].

In our work, the discretization of LBO $\Delta_{\mathcal{M}}$ is different from finite element method. With Lemma 2.5 in this document, we know that it is possible to approximate $\Delta_{\mathcal{M}} f(p)$ using integration. So we discretize the integration to approximate $\Delta_{\mathcal{M}} f(p)$ for each vertex p in point cloud P. The matrix form of this discretization is our discrete LBO $\hat{L}_P^t$. The convergence of $\hat{L}_P^t$ is shown in Theorem 4.2. Theorem 4.1 is about the convergence of Voronoi cell approximation. It is essential to the proof of Theorem 4.2. Proofs for these theorems are presented in section 1 of this document. Lemmas referred from existing works are presented in section 2 of this document. Miscellaneous lemmas are presented in section 3 and 4 of this document.

1 Convergence Proof

In our construction of PB-MHB, the assumption is we have a continuous differentiable Riemannian manifold $\mathcal{M}$ on which the sample set P lies. f is a C^2 continuous function defined over $\mathcal{M}$. We are going to prove that the result of our discrete LBO applied on the function $\hat{L}_P^t\mathbf{f}$ converges to the continuous result $\Delta_M f$ point-wisely.

To show the convergence of $\hat{L}_P^t$, first we are proving that our estimation of the Voronoi cell area is converging to the real Voronoi cell area as point clouds get denser. This part is proved in appendix section 1.1. After having the Voronoi cell area convergence result, we prove that $\hat{L}_P^t\mathbf{f}$ converges to $\Delta_M f$ point-wisely in appendix section 1.2.

1.1 Proof of Theorem 4.1: Convergence of Estimated Voronoi Cell Area

As shown in figure 1, the proof consists of two steps: (1) we prove that the projection of $Vr_{\mathcal{M}}(p)$ on the estimated tangent plane $\hat{T}_p$, $\hat{\Pi}(Vr_{\mathcal{M}}(p))$, has converging area to $Vr_{\mathcal{M}}(p)$, as shown in Lemma 1.5; (2) we build the upper bound and the lower bound of $\mathrm{vol}(\hat{\Pi}(Vr_{\mathcal{M}}(p)))$ that are both converging to $\mathrm{vol}(Vr_{\hat{T}}(p))$ so we know that $\mathrm{vol}(\hat{\Pi}(Vr_{\mathcal{M}}(p)))$ is converging to $\mathrm{vol}(Vr_{\hat{T}}(p))$. By combining this result with Lemma 1.5, we have Theorem 4.1 proved.

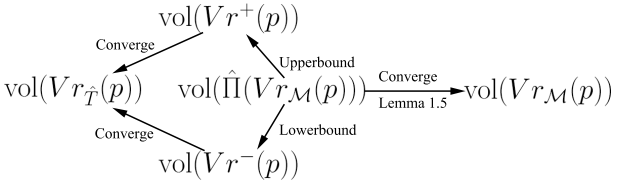

Fig. 1. Proof structure of Theorem 4.1.

To prove Lemma 1.5 we need to prove that there are some bounds on the sizes of the Voronoi cells $Vr_{\mathcal{M}}(p)$ and $Vr_{\hat{T}}(p)$ (Lemma 1.1 and Lemma 1.3), and there are some bounds on the set of neighboring points that may influence these Voronoi cells (Lemma 1.2 and Lemma 1.4).

***Lemma** 1.1 (Bound of $Vr_{\mathcal{M}}(p)$):* Consider the underlying manifold $\mathcal{M}$ and its ε-sampling P, $\forall p \in P$:

$$Vr_{\mathcal{M}}(p) \subseteq B(p, \varepsilon) \tag{1.1}$$

holds, i.e., its Voronoi cell on the manifold is bounded by a ball with radius ε.

Proof: Suppose $\exists q \in Vr_{\mathcal{M}}(p) \subseteq \mathcal{M}$, that satisfies $\|p-q\| > \varepsilon$.

$\because$ P is ε-sampling,

$\therefore$ There is another point $p' \in P$ that satisfies $\|p'-q\| \leq \varepsilon < \|p-q\|$, which means q is closer to p' instead of p.

$\therefore$ $q \notin Vr_{\mathcal{M}}(p)$. This is contradictory to assumption. □

***Lemma** 1.2 (Bound of Influencing Points on $\mathcal{M}$):* Consider the boundary of the Voronoi cell: $\partial Vr_{\mathcal{M}}(p)$. Given that P is an ε-sampling of $\mathcal{M}$, $\forall q \in \partial Vr_{\mathcal{M}}(p)$, $\exists p' \in P$, $p' \neq p$ satisfies $\|q-p\| = \|q-p'\|$, then for all such kind of points p',

$$\|p-p'\| \leq 2\varepsilon \tag{1.2}$$

holds. That is, only the point set in $B(p, 2\varepsilon)$ may influence the Voronoi cell of point p.

Proof: According to Lemma 1.1, we have $\|q-p\| \leq \varepsilon$ and $\|q-p'\| \leq \varepsilon$ hold for $\forall q \in \partial Vr_{\mathcal{M}}(p)$. Thus we have

$$\|p-p'\| \leq \|q-p\| + \|q-p'\| \leq \varepsilon + \varepsilon = 2\varepsilon. \tag{1.3}$$

□

As described in the paper, we project a local neighborhood of points $P_\delta = P \cap B(p,\delta)$, $\delta \geq 10\varepsilon$ onto the estimated tangent plane $\hat{T}_p$. When δ, ε and $r/\rho = 10\varepsilon/\rho$ are small enough, the projection from the local patch $\mathcal{M} \cap B(p,\delta)$ to $\hat{T}_p$, denoted as $\hat{\Pi}$, is bijective. Let $\hat{\Phi} = \hat{\Pi}^{-1}$.

***Lemma** 1.3 (Bound of $Vr_{\hat{T}}(p)$):* Consider the Voronoi diagram of $p \cup \{\hat{\Pi}(P_\delta - p)\}$ on $\hat{T}_p$, where $p \in P$ is a sample point and P is an ε-sampling of $\mathcal{M}$. Denote the Voronoi cell of p on $\hat{T}_p$ as $Vr_{\hat{T}}(p)$, then

$$Vr_{\hat{T}}(p) \subseteq B(p,\varepsilon) \tag{1.4}$$

holds. That is, $Vr_{\hat{T}}(p)$ is bounded by a ball with radius ε.

Proof:

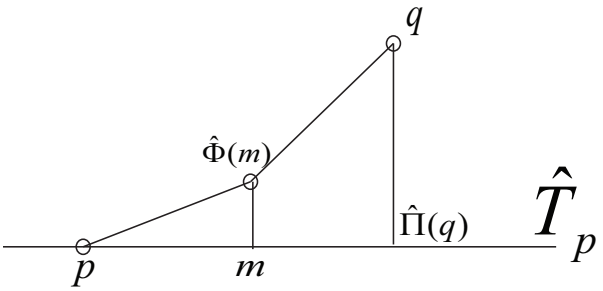

Fig. 2. Bound of $Vr_{\hat{T}}(p)$ for Lemma 1.3.

Suppose $\exists m \in Vr_{\hat{T}}(p)$ and $\|p-m\| > \varepsilon$, as shown in figure 2.

$\because m \in Vr_{\hat{T}}(p)$,

$\therefore \forall q \in P$ and $p \neq q$, $\|\hat{\Pi}(q) - m\| \geq \|p-m\| > \varepsilon$.

Here $p = \hat{\Pi}(p)$ since p lies on both $\mathcal{M}$ and $\hat{T}_p$.

$\because \hat{\Pi}$ is the projection from $\mathcal{M}$ to $\hat{T}_p$ and $\hat{\Phi} = \hat{\Pi}^{-1}$,

$\therefore \|p-m\| \leq \|p - \hat{\Phi}(m)\|$, $\|\hat{\Pi}(q) - m\| \leq \|q - \hat{\Phi}(m)\|$,

$\therefore \forall q \in P, \|q - \hat{\Phi}(m)\| \geq \|\hat{\Pi}(q) - m\| > \varepsilon$. This is contradictory to the assumption that P is ε-sampled.

□

***Lemma** 1.4 (Bound of Influencing Points on $\hat{T}_p$):* Consider the boundary of the Voronoi cell on the estimated tangent plane: $\partial Vr_{\hat{T}}(p)$. Given that P is an ε-sampling of $\mathcal{M}$, $\forall q \in \partial Vr_{\hat{T}}(p)$, $\exists p' \in P$, $p' \neq p$ satisfies $\|q-p\| = \|q - \hat{\Pi}(p')\|$, then for all such kind of points p',

$$\|p - \hat{\Pi}(p')\| \leq 2\varepsilon \tag{1.5}$$

holds. That is, only the projected sample points in $B(p, 2\varepsilon)$ may influence the Voronoi cell $Vr_{\hat{T}}(p)$.

Proof: According to Lemma 1.3, we know that $\forall q \in \partial Vr_{\hat{T}}(p)$, $\|p-q\| \leq \varepsilon$.

Thus for the influencing projected point $\hat{\Pi}(p')$ we have

$$\|p-q\| = \|q - \hat{\Pi}(p')\| \tag{1.6}$$
$$\|p - \hat{\Pi}(p')\| \leq \|p-q\| + \|q - \hat{\Pi}(p')\| \tag{1.7}$$
$$\leq \varepsilon + \varepsilon = 2\varepsilon \tag{1.8}$$

□

***Lemma** 1.5 (Convergence of $\hat{\Pi}(Vr_{\mathcal{M}}(p))$ to $Vr_{\mathcal{M}}(p)$):* Consider projecting $Vr_{\mathcal{M}}(p)$ to $\hat{T}_p$. P is an ε-sampling of $\mathcal{M}$, and ρ is the local feature size of point $p \in P$. Then

$$\left\| \frac{\mathrm{vol}(Vr_{\mathcal{M}}(p))}{\mathrm{vol}(\hat{\Pi}(Vr_{\mathcal{M}}(p)))} - 1 \right\| = O(\frac{\varepsilon^2}{\rho^2}) \tag{1.9}$$

holds.

Proof:

$\forall q \in Vr_{\mathcal{M}}(p)$, consider the angle $\angle(T_q, \hat{T}_p)$ between the two planes T_q and $\hat{T}_p$, where T_p and T_q are the real tangent planes of $\mathcal{M}$ at points p and q, $\hat{T}_p$ is the estimated tangent plane at point p, as described in the paper.

According to Lemma 2.1 (in appendix section 2), when $\|p-q\| < \rho/3$ we have

$$\angle(T_p, T_q) \leq \frac{\|p-q\|}{\rho - \|p-q\|} \leq O(\varepsilon/\rho). \tag{1.10}$$

We get the last inequality by applying Lemma 1.1.

Now we have three planes here: T_p, T_q and $\hat{T}_p$. According to Lemma 4.1 (in appendix section 4), when all angles are small,

$$\angle(T_q, \hat{T}_p) \leq \angle(T_p, T_q) + \angle(T_p, \hat{T}_p)$$
$$\leq O(\varepsilon/\rho) \tag{1.11}$$

holds, where we get the second inequality by applying Lemma 2.3 (in appendix section 2). Thus we have:

$$\cos\angle(T_q, \hat{T}_p) = \sqrt{1 - \sin^2\angle(T_q, \hat{T}_p)} \tag{1.12}$$
$$\geq \sqrt{1 - (\angle(T_q, \hat{T}_p))^2} \tag{1.13}$$
$$\geq \sqrt{1 - O(\varepsilon^2/\rho^2)} \tag{1.14}$$
$$\geq 1 - O(\varepsilon^2/\rho^2). \tag{1.15}$$

When δ, ε and $r/\rho = 10\varepsilon/\rho$ are small enough, the projection from the local patch $\mathcal{M} \cap B(p,\delta)$ to $\hat{T}_p$, denoted as $\hat{\Pi}$, is bijective. Denote $\gamma = \angle(T_q, \hat{T}_p)$, then we have

$$\mathrm{vol}(Vr_{\mathcal{M}}(p)) = \int_{q \in \hat{\Pi}(Vr_{\mathcal{M}}(p))} \frac{1}{\cos\gamma} ds \tag{1.16}$$
$$\leq \max(\frac{1}{\cos\gamma}) \int_{q \in \hat{\Pi}(Vr_{\mathcal{M}}(p))} ds \tag{1.17}$$
$$= \max(\frac{1}{\cos\gamma})\, \mathrm{vol}(\hat{\Pi}(Vr_{\mathcal{M}}(p))). \tag{1.18}$$

Thus by combining (1.18) with (1.15), we can have

$$1 \leq \left\| \frac{\mathrm{vol}(Vr_{\mathcal{M}}(p))}{\mathrm{vol}(\hat{\Pi}(Vr_{\mathcal{M}}(p)))} \right\| \leq \frac{1}{\min(\cos\gamma)} \leq 1 + O(\varepsilon^2/\rho^2). \tag{1.19}$$

□

With these results we can prove Theorem 4.1 as follows:

Proof:

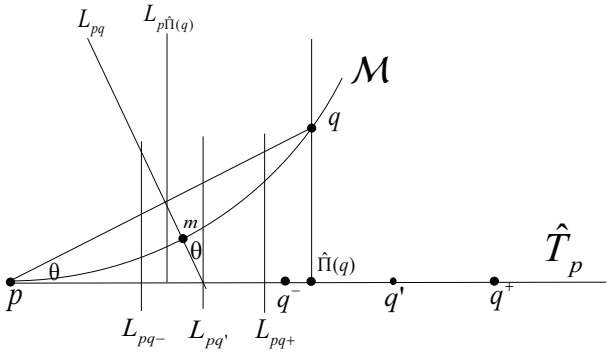

Fig. 3. Parallel bisecting planes.

As described in the paper, we chose the neighboring points $P_\delta = P \cap B(p,\delta)$, $\delta \geq 10\varepsilon$ for projection. According to Lemma 1.4, for $Vr_{\hat{T}}(p)$, any influencing projected point $q \in P_\delta$ satisfies $\|\hat{\Pi}(q) - p\| \leq 2\varepsilon$. Consider $\forall q \in P_\delta$, according to Lemma 2.2, 2.3 and 4.2, we have $\angle(pq, \hat{T}_p)) \leq \angle(pq, T_p) + \angle(\hat{T}_p, T_p) = O(\frac{\|p-q\|}{\rho}) + O(r/\rho)$ and $\frac{\|p-q\|}{\|p-\hat{\Pi}(q)\|} - 1 = O(\frac{\varepsilon}{\rho}) + O(\frac{\|p-q\|}{\rho})$. When ε is small enough, we have $(\hat{T}_p \cap B(p, 2\varepsilon)) \subseteq \hat{\Pi}(\mathcal{M} \cap B(p,r))$. Thus we know for $\forall q \in P_\delta$ that satisfies $\|p - \hat{\Pi}(q)\| \leq 2\varepsilon$, $\|p - q\| \leq r = 10\varepsilon$ holds. That is, all neighboring points that could influence $Vr_{\hat{T}}(p)$ are included in $P_r = P \cap B(p,r)$. According to Lemma 1.2, we know that all points which may influence $Vr_{\mathcal{M}}(p)$ are also included in P_r.

On the estimated tangent plane $\hat{T}_p$, we are building 4 sets of Voronoi diagrams to get the converging approximation of the Voronoi cell area, as shown in Fig. 3.

For each point $q \in P_\delta$, $q \neq p$, we consider the bisecting plane L_{pq} between points p and q. We also build the bisecting plane $L_{p\hat{\Pi}(q)}$ for the point-pair $\{p, \hat{\Pi}(q)\}$. As shown in Fig. 3, it is obvious that $L_{p\hat{\Pi}(q)} \perp \hat{T}_p$, and the straight line $l_{p\hat{\Pi}(q)} = L_{p\hat{\Pi}(q)} \cap \hat{T}_p$ is also the bisecting line on $\hat{T}_p$ for the point-pair $\{p, \hat{\Pi}(q)\}$. $\{l_{p\hat{\Pi}(q)}\}$ are also the lines that compose $\partial Vr_{\hat{T}}(p)$, which is the boundary of the Voronoi cell of p on $\hat{T}_p$. Notice that for some points $q \in P_\delta$, $l_{p\hat{\Pi}(q)} \cap \partial Vr_{\hat{T}}(p) = \emptyset$. That is, it is not necessary that all bisecting lines contribute to the boundary of $Vr_{\hat{T}}(p)$.

Consider the lines $l_{pq} = L_{pq} \cap \hat{T}_p$. Since we have $q\hat{\Pi}(q) \perp \hat{T}_p$ and $pq \perp L_{pq}$, we know that $l_{pq} \perp pq$ and $l_{pq} \perp q\hat{\Pi}(q)$. Thus $l_{pq} \perp p\hat{\Pi}(q)$. Because $L_{p\hat{\Pi}(q)} \perp p\hat{\Pi}(q)$, we know that $l_{pq} \parallel L_{p\hat{\Pi}(q)}$. Then for each l_{pq}, we can build the plane $L_{pq'}$ satisfying $l_{pq} \subset L_{pq'}$ and $L_{pq'} \parallel L_{p\hat{\Pi}(q)}$.

As shown in Fig. 3, we denote $\theta = \angle(L_{p\hat{\Pi}(q)}, L_{pq})$. According to Lemma 4.2 (in appendix section 4), we have

$$\theta = \angle(L_{p\hat{\Pi}(q)}, L_{pq}) \tag{1.20}$$
$$= \angle(p\hat{\Pi}(q), pq) \tag{1.21}$$
$$\leq \angle(pq, T_p) + \angle(T_p, \hat{T}_p). \tag{1.22}$$

According to lemma 2.2 (in appendix section 2), we have

$$\sin\angle(pq, T_p) \leq O(\frac{\varepsilon}{\rho}). \tag{1.23}$$

According to lemma 2.3 (in appendix section 2), we have

$$\angle(T_p, \hat{T}_p) \leq O(\frac{r}{\rho}). \tag{1.24}$$

By combining (1.23), (1.24) with (1.22), we have

$$\sin\theta \leq O(\frac{r}{\rho}) + O(\frac{\varepsilon}{\rho}), \tag{1.25}$$
$$\tan\theta = \frac{\sin\theta}{\cos\theta} \tag{1.26}$$
$$\leq O\left(\frac{(\varepsilon+r)/\rho}{\sqrt{1-(\varepsilon+r)^2/\rho^2}}\right) \tag{1.27}$$
$$\leq O\left(\frac{\varepsilon+r}{\sqrt{\rho^2-(\varepsilon+r)^2}}\right) \tag{1.28}$$
$$\leq O\left(\frac{\varepsilon+r}{\rho-\varepsilon-r}\right). \tag{1.29}$$

We consider the points on the Voronoi cell boundaries: $m \in \partial Vr_{\mathcal{M}}(p)$, as shown in Fig. 3. According to Lemma 2.2, we have $\sin(\angle(pm, T_p)) \leq O(\varepsilon/\rho)$, since $\|p - m\| \leq \varepsilon$ from Lemma 1.1. When all angles are small, we have

$$\sin(\angle(pm, \hat{T}_p)) \tag{1.30}$$
$$\leq \sin(\angle(pm, T_p) + \angle(T_p, \hat{T}_p)) \tag{1.31}$$
$$\leq \sin(\angle(pm, T_p)) + \sin(\angle(T_p, \hat{T}_p)) \tag{1.32}$$
$$\leq \sin(\angle(pm, T_p)) + \angle(T_p, \hat{T}_p) \tag{1.33}$$
$$\leq \frac{\varepsilon}{2\rho} + \frac{r}{\rho} \tag{1.34}$$
$$\leq O(\frac{\varepsilon}{\rho}) \tag{1.35}$$

holds since we have $r = 10\varepsilon$. Then we have the bound of the distance from m to $\hat{T}_p$:

$$d(m, \hat{T}_p) \leq \varepsilon \cdot \sin(\angle(pm, \hat{T}_p)) \leq O(\varepsilon^2/\rho). \tag{1.36}$$

Suppose $q \in P_\delta$, $q \neq p$ is the influencing point for $m \in \partial Vr_{\mathcal{M}}(p)$, i.e., $\|p - m\| = \|q - m\|$. By combining (1.29) with (1.36), we have the bound of the distance from m to the plane $L_{pq'}$:

$$d(m, L_{pq'}) = \tan\theta \cdot d(m, \hat{T}_p) \tag{1.37}$$
$$\leq O\left(\frac{\varepsilon+r}{\rho-\varepsilon-r}\right) \cdot O(\frac{\varepsilon^2}{\rho}) \tag{1.38}$$
$$\leq O\left(\frac{\varepsilon^2(\varepsilon+r)}{\rho(\rho-\varepsilon-r)}\right). \tag{1.39}$$

That is, $\exists c \in \mathbb{R}$, $c > 0$, $d(m, L_{pq'}) \leq c \cdot \frac{\varepsilon^2(\varepsilon+r)}{\rho(\rho-\varepsilon-r)}$.

Next we build 2 planes for each $q \in P_\delta$, $q \neq p$: L_{pq+} and L_{pq-} that satisfy $L_{pq+} \parallel L_{p\hat{\Pi}(q)} \parallel L_{pq-}$, and

$$d(L_{pq+}, L_{pq'}) = d(L_{pq-}, L_{pq'}) \tag{1.40}$$

$$= c \cdot \frac{\varepsilon^2(\varepsilon+r)}{\rho(\rho-\varepsilon-r)}, \tag{1.41}$$

$$d(p, L_{pq-}) \leq d(p, L_{pq'}) \leq d(p, L_{pq+}). \tag{1.42}$$

Since $L_{p\hat{\Pi}(q)} \perp \hat{T}_p$, we know that $L_{pq+} \perp \hat{T}_p$, $L_{pq-} \perp \hat{T}_p$. As shown in Fig. 3, we also have

$$d(p, L_{pq'}) = \frac{\|p-q\|}{2\cos\theta} \tag{1.43}$$

As shown in Fig. 3, we build the points q', q^+, q^- according to $L_{pq'}$, L_{pq+} and L_{pq-}, so that these planes are the bisecting planes between the point-pairs $\{p, q'\}$, $\{p, q^+\}$ and $\{p, q^-\}$, respectively.

It is obvious that q', q^+, q^- reside on the same line of $p\hat{\Pi}(q)$. Then we can build the Voronoi diagrams over $\hat{T}_p$ with points $\{p\} \cup \{q^+\}$, $\{p\} \cup \{q'\}$ and $\{p\} \cup \{q^-\}$. Denote the Voronoi cell of p of these diagrams as $Vr^+(p)$, $Vr'(p)$ and $Vr^-(p)$. According to Lemma 1.2 and Lemma 1.4, we can ignore other points $q \notin P_\delta$ without affecting these Voronoi cells for p. Thus we will only use points $q \in P_\delta$, $q \neq p$.

Since the point cloud P is an $(\varepsilon, s\varepsilon)$-sample of $\mathcal{M}$, we have $s\varepsilon \leq \|p-q\| \leq 10\varepsilon$. When ε is small enough, we always have $c \cdot \frac{\varepsilon^2(\varepsilon+r)}{\rho(\rho-\varepsilon-r)} < O(\varepsilon) \leq \frac{\|p-q\|}{2\cos\theta}$. Thus p will not stay in between L_{pq-} and L_{pq+}. Then we can have:

$$\|p - \hat{\Pi}(q)\| = \|p-q\| \cdot \cos\theta, \tag{1.44}$$

$$\|p - q'\| = 2 \cdot d(p, L_{pq'}) = \|p-q\| / \cos\theta, \tag{1.45}$$

$$\|p - q^+\| = \|p-q\| / \cos\theta + 2 \cdot c \cdot \frac{\varepsilon^2(\varepsilon+r)}{\rho(\rho-\varepsilon-r)}, \tag{1.46}$$

$$\|p - q^-\| = \|p-q\| / \cos\theta - 2 \cdot c \cdot \frac{\varepsilon^2(\varepsilon+r)}{\rho(\rho-\varepsilon-r)}. \tag{1.47}$$

For $\forall m \in \partial Vr_{\mathcal{M}}(p) \cap L_{pq}$ and its corresponding influencing point q, we have

$$d(m, L_{pq'}) \leq d(L_{pq-}, L_{pq'}), \tag{1.48}$$

$$d(m, L_{pq'}) \leq d(L_{pq+}, L_{pq'}), \tag{1.49}$$

$$\|m-p\| = \|m-q\|. \tag{1.50}$$

So we know that m stays in between L_{pq-} and L_{pq+} of point q. This can lead to:

$$\|m-p\| \leq \|m-q^+\|, \tag{1.51}$$

$$\|m-p\| \geq \|m-q^-\|. \tag{1.52}$$

Recall that here q is the influencing point of $m \in \partial Vr_{\mathcal{M}}(p)$. Since $\hat{\Pi}$ is bijective projection, it is obvious that $\hat{\Pi}(\partial Vr_{\mathcal{M}}(p)) = \partial\hat{\Pi}(Vr_{\mathcal{M}}(p))$. So we have $\forall \hat{m} \in \partial\hat{\Pi}(Vr_{\mathcal{M}}(p))$, $\exists q \in P_\delta$, such that $\|\hat{m}-p\| \geq \|\hat{m}-q^-\|$. This means that $\partial\hat{\Pi}(Vr_{\mathcal{M}}(p)) \cap (Vr^-(p) - \partial Vr^-(p)) = \emptyset$.

$$\because p \in Vr^-(p), p \in \hat{\Pi}(Vr_{\mathcal{M}}(p)),$$
$$\therefore Vr^-(p) \subseteq \hat{\Pi}(Vr_{\mathcal{M}}(p)). \tag{1.53}$$

Let us assume that $\hat{\Pi}(Vr_{\mathcal{M}}(p)) \subseteq Vr^+(p)$ does not hold, then $\exists m \in (Vr_{\mathcal{M}}(p))$, such that $\|\hat{\Pi}(m) - p\| > \|\hat{\Pi}(m) - q^+\|$ for some $q \in P_\delta$. As shown in Fig. 3, m resides in the p-side of plane L_{pq}. Since m also resides on the q^+-side of plane L_{pq+}, we have $\min d(m, \hat{T}_p) > d(L_{pq'}, L_{pq+}) \cdot \cot\theta$. Recall that we construct L_{pq+} so that $d(L_{pq'}, L_{pq+}) \geq \max d(m', \hat{T}_p) \cdot \tan\theta$ for $\forall m' \in Vr_{\mathcal{M}}(p)$. Thus we have $\min d(m, \hat{T}_p) > \max d(m', \hat{T}_p)$ for $\forall m' \in Vr_{\mathcal{M}}(p)$. Thus we have $m \notin Vr_{\mathcal{M}}(p)$, which is contradictory to the assumption. So we have $\hat{\Pi}(Vr_{\mathcal{M}}(p)) \subseteq Vr^+(p)$ holds.

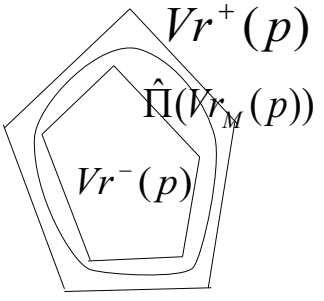

Fig. 4. The nestling of $Vr^-(p)$, $Vr^+(p)$, and $\hat{\Pi}(Vr_{\mathcal{M}}(p))$.

As shown in Fig. 4, we have

$$Vr^-(p) \subseteq \hat{\Pi}(Vr_{\mathcal{M}}(p)) \subseteq Vr^+(p), \tag{1.54}$$

which means that:

$$\mathrm{vol}(Vr^-(p)) \leq \mathrm{vol}(\hat{\Pi}(Vr_{\mathcal{M}}(p))) \leq \mathrm{vol}(Vr^+(p)). \tag{1.55}$$

Since we have $s\varepsilon \leq \|p-q\| \leq r = 10\varepsilon$, by combining equations (1.44), (1.45), (1.46), and (1.47), we can have

$$\frac{\|p-q^+\|}{\|p-q'\|} \leq 1 + O(\varepsilon^2/\rho^2), \tag{1.56}$$

$$\frac{\|p-q^-\|}{\|p-q'\|} \geq 1 - O(\varepsilon^2/\rho^2), \tag{1.57}$$

$$\frac{\|p-q'\|}{\|p-\hat{\Pi}(q)\|} = \frac{1}{\cos^2\theta} \leq 1 + O(\varepsilon^2/\rho^2). \tag{1.58}$$

We get the above last equation from Lemma 1.2 and similar calculation as in equation (1.35). According to Lemma 3.3 (in appendix section 3), we have

$$\left\| \frac{\mathrm{vol}(Vr^+(p))}{\mathrm{vol}(Vr'(p))} - 1 \right\| \leq O(\varepsilon^2/\rho^2), \tag{1.59}$$

$$\left\| \frac{\mathrm{vol}(Vr^-(p))}{\mathrm{vol}(Vr'(p))} - 1 \right\| \leq O(\varepsilon^2/\rho^2), \tag{1.60}$$

$$\left\| \frac{\mathrm{vol}(Vr'(p))}{\mathrm{vol}(Vr_{\hat{T}}(p))} - 1 \right\| \leq O(\varepsilon^2/\rho^2). \tag{1.61}$$

Finally we have

$$\left\| \frac{\mathrm{vol}(\hat{\Pi}(Vr_{\mathcal{M}}(p)))}{\mathrm{vol}(Vr_{\hat{T}}(p))} - 1 \right\| \leq O(\varepsilon^2/\rho^2). \tag{1.62}$$

By combining equation (1.62) with Lemma 1.5, we have

$$\left\| \frac{\mathrm{vol}(Vr_{\mathcal{M}}(p))}{\mathrm{vol}(Vr_{\hat{T}}(p))} - 1 \right\| \leq O(\varepsilon^2/\rho^2). \tag{1.63}$$

□

1.2 Proof of Theorem 4.2: Convergence of Integration Approximation

$$\hat{\Delta}_P^t \xrightarrow{\text{Converge}} \check{\Delta}_P^t \xrightarrow[\text{Lemma 1.9}]{\text{Converge}} \Delta_{\mathcal{M}}$$

Fig. 5. Proof structure of Theorem 4.2.

As shown in figure 5, the proof of Theorem 4.2 is organized as follows: An intermediate discrete LBO $\check{\Delta}_P^t$ is defined first in equation (1.64). $\check{\Delta}_P^t$ is the approximation result by computing the integration directly over the manifold. In Lemma 1.9 we show that $\check{\Delta}_P^t$ is converging to $\Delta_{\mathcal{M}}$. With the Voronoi cell area convergence result in Theorem 4.1, we then show that our discrete LBO $\hat{\Delta}_P^t$ (with Voronoi cell area estimated on the tangent plane) is converging to $\check{\Delta}_P^t$, which means that $\hat{\Delta}_P^t$ is converging to $\Delta_{\mathcal{M}}$ as well.

Recall that in our algorithm, the approximation LBO $\hat{\Delta}_P^t$ is defined as:

$$\hat{\Delta}_P^t f(p) = \frac{1}{4\pi t^2} \sum_{q \in P_\delta} (e^{-\frac{\|q-p\|^2}{4t}} (f(q) - f(p)) \,\mathrm{vol}(Vr_{\hat{T}}(q))),$$

where $Vr_{\hat{T}}(q)$ is the Voronoi cell of the point q over $\hat{T}_q$. In order to prove that $\hat{\Delta}_P^t$ is converging to the LBO $\Delta_{\mathcal{M}}$, we introduce the following intermediate LBO:

$$\check{\Delta}_P^t f(p) = \frac{1}{4\pi t^2} \sum_{q \in P_\delta} (e^{-\frac{\|q-p\|^2}{4t}} (f(q) - f(p)) \,\mathrm{vol}(Vr_{\mathcal{M}}(q))). \tag{1.64}$$

It is obvious that the only difference between $\hat{\Delta}_P^t$ and $\check{\Delta}_P^t$ is that we use $Vr_{\hat{T}}(q)$ instead of $Vr_{\mathcal{M}}(q)$ as in (1.64), because it is impossible to get $\mathrm{vol}(Vr_{\mathcal{M}}(q))$ in most real applications.

***Definition** 1.6:* For $\forall p \in P$, recall we have $P_\delta = P \cap B(p, \delta)$. Define

$$N_p = \mathcal{M} \cap B(p, \delta) \tag{1.65}$$
$$N_{Vp} = \cup_{q \in P_\delta} Vr_{\mathcal{M}}(q) \tag{1.66}$$
$$N_p^+ = \mathcal{M} \cap B(p, 1.1\delta) \tag{1.67}$$
$$N_p^- = \mathcal{M} \cap B(p, 0.9\delta) \tag{1.68}$$

given $\delta \geq 10\varepsilon$.

According to Lemma 2.5, the continuous LBO $\Delta_{\mathcal{M}}$ can be computed as the integration over the whole manifold $\mathcal{M}$. Our essential idea is to approximate such integration locally over N_{Vp} instead. And the following Lemma 1.8 shows that such local approximation is reasonable, which can lead to the convergence of $\check{\Delta}_P^t$ to $\Delta_{\mathcal{M}}$, as shown in Lemma 1.9. In order to prove Lemma 1.8, we need to show that N_{Vp} is bounded in between N_p^- and N_p^+ which are independent of the sampling size ε, which is addressed in the following Lemma 1.7.

***Lemma** 1.7 (Bound of N_{Vp}):*

$$N_p^- \subseteq N_{Vp} \subseteq N_p^+. \tag{1.69}$$

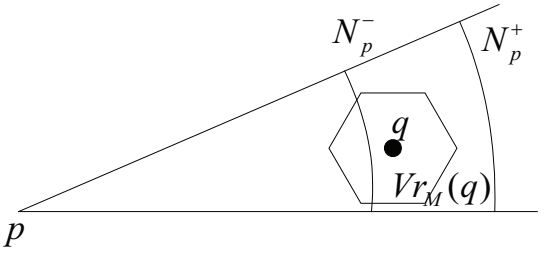

Fig. 6. The nestling of N_p^-, N_p^+, and N_{Vp}.

Proof: This nestling relationship is shown in Figure 6.

First we prove $N_p^- \subseteq N_{Vp}$: For $\forall m \in N_p^-$, there exists $\exists q \in P$, such that $m \in Vr_{\mathcal{M}}(q)$. According to Lemma 1.1, we have $\|q - m\| \leq \varepsilon$.

$\because \|p - q\| \leq \|p - m\| + \|q - m\| \leq 0.9\delta + \varepsilon \leq \delta$,

$\therefore q \in P_\delta$, $Vr_{\mathcal{M}}(q) \subseteq N_{Vp}$, $m \in N_{Vp}$.

Next we prove $N_{Vp} \subseteq N_p^+$: For $\forall m \in N_{Vp}$, there exists $\exists q \in P_\delta$, $m \in Vr_{\mathcal{M}}(q)$. Recall that $\|q - m\| \leq \varepsilon$ and $\|p - q\| \leq \delta$, so we have $\|p - m\| \leq \|p - q\| + \|q - m\| \leq \delta + \varepsilon \leq 1.1\delta$. Thus $m \in N_p^+$. □

***Lemma** 1.8 (Approximation using N_{Vp}):*

$$\int_{N_{Vp}} e^{-\frac{\|p-y\|}{4t}} f(y) d\mu_y - \int_{\mathcal{M}} e^{-\frac{\|p-y\|}{4t}} f(y) d\mu_y = o(t^l), \tag{1.70}$$

for any positive natural number l.

Proof: Similar to the proof of Lemma 2.4(in this material), which is Lemma 1 in [4]:

$$\begin{aligned}
&\left| \int_{N_{Vp}} e^{-\frac{\|p-y\|}{4t}} f(y) d\mu_y - \int_{\mathcal{M}} e^{-\frac{\|p-y\|}{4t}} f(y) d\mu_y \right| \\
=&\left| \int_{\mathcal{M} - N_{Vp}} e^{-\frac{\|p-y\|}{4t}} f(y) d\mu_y \right| \\
\leq& \,\mathrm{vol}(\mathcal{M}) \sup_{x \in \mathcal{M}, x \notin N_{Vp}} (|f(x)|) e^{-\frac{d_1^2}{4t}} \qquad (1.71) \\
\leq& \,\mathrm{vol}(\mathcal{M}) \sup_{x \in \mathcal{M}, x \notin N_p^-} (|f(x)|) e^{-\frac{d_2^2}{4t}} = o(t^l), \qquad (1.72)
\end{aligned}$$

where $d_1 = \inf_{x \notin N_{Vp}} \|p - x\|$, and $d_2 = \inf_{x \notin N_p^-} \|p - x\|$. □

***Lemma** 1.9 (Convergence of $\check{\Delta}_P^t$ to $\Delta_{\mathcal{M}}$):*

$$\lim_{\varepsilon\to 0}\|\check{\Delta}_P^t f-\Delta_{\mathcal{M}} f\|_\infty=0, \tag{1.73}$$

where $t(\varepsilon)=\varepsilon^{\frac{1}{2+\xi}}$, and $\xi>0$ is any positive fixed number.

Proof: Note that $\varepsilon=t^{2+\xi}$. According to Lemma 1.1, we know $\forall y\in Vr_{\mathcal{M}}(q)$, $\|y-q\|\le\varepsilon$ or $\|y-q\|\le O(\varepsilon)$. According to Lemma 2.5, we can approximate $\Delta_{\mathcal{M}}$ using integration over $\mathcal{M}$. Thus we have:

$$\lim_{t\to 0}\left|\check{\Delta}_P^t f(p)-\int_{N_{Vp}} e^{-\frac{\|p-y\|^2}{4t}}(f(y)-f(p))d\mu_y\right| \tag{1.74}$$

$$=\lim_{t\to 0}|\sum_{q\in P_\delta}\int_{Vr_{\mathcal{M}}(q)}\frac{1}{4\pi t^2}[e^{-\frac{\|q-p\|^2}{4t}}(f(q)-f(p)) - e^{-\frac{\|y-p\|^2}{4t}}(f(y)-f(p))]d\mu_y| \tag{1.75}$$

$$=\lim_{t\to 0}|\sum_{q\in P_\delta}\int_{Vr_{\mathcal{M}}(q)}\frac{1}{4\pi t^2}[e^{-\frac{\|q-p\|^2}{4t}}(f(q)-f(p))-e^{-\frac{\|q-p\|^2}{4t}}(f(y)-f(p)) + e^{-\frac{\|q-p\|^2}{4t}}(f(y)-f(p))-e^{-\frac{\|y-p\|^2}{4t}}(f(y)-f(p))]d\mu_y| \tag{1.76}$$

$$=\lim_{t\to 0}|\sum_{q\in P_\delta}\int_{Vr_{\mathcal{M}}(q)}\frac{1}{4\pi t^2}e^{-\frac{\|y-p\|^2}{4t}}[e^{\frac{\|y-p\|^2-\|q-p\|^2}{4t}}(f(q)-f(y)) + (e^{\frac{\|y-p\|^2-\|q-p\|^2}{4t}}-1)(f(y)-f(p))]d\mu_y| \tag{1.77}$$

$$\le\lim_{t\to 0}\sum_{q\in P_\delta}\int_{Vr_{\mathcal{M}}(q)}\frac{1}{4\pi t^2}e^{-\frac{\|y-p\|^2}{4t}}[|f(y)-f(p)|\cdot \left|e^{-\frac{O(\varepsilon)}{4t}}-1\right|+O(\varepsilon)]d\mu_y \tag{1.78}$$

$$\le\lim_{t\to 0}\frac{(f_{\max,\mathcal{M}}-f_{\min,\mathcal{M}})\cdot\left|e^{-\frac{O(\varepsilon)}{4t}}-1\right|+O(\varepsilon)}{t} \cdot\int_{N_{Vp}}\frac{1}{4\pi t}e^{-\frac{\|y-p\|^2}{4t}}d\mu_y \tag{1.79}$$

$$\le\lim_{t\to 0}\frac{(f_{\max,\mathcal{M}}-f_{\min,\mathcal{M}})\left|e^{-\frac{O(\varepsilon)}{4t}}-1\right|+O(\varepsilon)}{t} \cdot\text{Constant} \tag{1.80}$$

$$\le\lim_{t\to 0}\frac{O(\varepsilon/t)+O(\varepsilon)}{t} \tag{1.81}$$

$$=\lim_{t\to 0}\frac{O(t^{1+\xi})+O(t^{2+\xi})}{t}=0 \tag{1.82}$$

where $f_{\max,\mathcal{M}}$ and $f_{\min,\mathcal{M}}$ stands for the maximum and minimum of function f on manifold $\mathcal{M}$. In the above derivation, we applied $\|q-p\|-\|y-q\|\le\|y-p\|\le\|q-p\|+\|y-q\|$, $\|y-q\|\le\varepsilon$, $|f(y)-f(q)|=O(|y-q|)$ (since $f\in C^2$) and following inequality on equation (1.77) to get equation (1.78).

$$\left|\|y-p\|^2-\|q-p\|^2\right| \tag{1.83}$$

$$=|(\|y-p\|+\|q-p\|)\cdot(\|y-p\|-\|q-p\|)| \tag{1.84}$$

$$\le(\|y-p\|+\|q-p\|)\cdot\varepsilon \tag{1.85}$$

$$\le(2\|q-p\|+\|y-q\|)\cdot\varepsilon \tag{1.86}$$

$$\le(2\|q-p\|+\varepsilon)\cdot\varepsilon \tag{1.87}$$

$$\le 2\delta\cdot\varepsilon+\varepsilon^2\le O(\varepsilon). \tag{1.88}$$

By applying the following inequality to equation (1.79), we get equation (1.80).

$$\int_{N_{Vp}}\frac{1}{4\pi t}e^{-\frac{\|y-p\|^2}{4t}}d\mu_y \tag{1.89}$$

$$=\int_{\hat{\Pi}(N_{Vp})}\frac{1}{4\pi t}e^{-\frac{\|\hat{\Phi}(y)-p\|^2}{4t}}|J(\hat{\Phi})|_y d\mu_y \tag{1.90}$$

$$\le\int_{\hat{\Pi}(N_{Vp})}\frac{1}{4\pi t}e^{-\frac{\|y-p\|^2}{4t}}|J(\hat{\Phi})|_y d\mu_y \tag{1.91}$$

$$\le\max_{y\in\hat{\Pi}(N_p^+)}(|J(\hat{\Phi})|_y)\int_{\hat{T}_p}\frac{1}{4\pi t}e^{-\frac{\|y-p\|^2}{4t}}d\mu_y \tag{1.92}$$

$$\le\max_{y\in\hat{\Pi}(N_p^+)}(|J(\hat{\Phi})|_y)=\text{Constant}. \tag{1.93}$$

Here J stands for the Jacobian Matrix.

By combining Lemma 2.5 and Lemma 1.8 (in this material) with equation (1.82), we have $\lim_{\varepsilon\to 0}\|\check{\Delta}_P^t f-\Delta_{\mathcal{M}} f\|_\infty=0$ proved. □

With Lemma 1.9, we can prove Theorem 4.2 as follows:

Proof:

According to Theorem 4.1, we have

$$\left\|\frac{\text{vol}(Vr_{\mathcal{M}}(p))}{\text{vol}(Vr_{\hat{T}}(p))}-1\right\|=O(\frac{\varepsilon^2}{\rho^2}). \tag{1.94}$$

Thus:

$$\left\|\frac{\check{\Delta}_P^t f(p)}{\hat{\Delta}_P^t f(p)}-1\right\|=O(\frac{\varepsilon^2}{\rho^2}), \tag{1.95}$$

which means:

$$\lim_{t\to 0}\|\check{\Delta}_P^t f(p)-\hat{\Delta}_P^t f(p)\|_\infty=0. \tag{1.96}$$

By combining (1.96) with Lemma 1.9, we have this theorem proved. □

2 Referred Lemmas

This appendix section shows the Lemmas that we referred from other papers. These Lemmas are used in our proof of convergence in appendix section 1.

***Lemma** 2.1 (Lemma 3.1 in [5]):* Given two points $p,q\in\mathcal{M}$ with $\|p-q\|\le\rho/3$, the angle between their normals n_p and n_q satisfies $\angle(n_p,n_q)<\frac{\|p-q\|}{\rho-\|p-q\|}$.

***Lemma** 2.2 (Lemma 6 in [6]):* For any point $p,q\in\mathcal{M}$ with $\|p-q\|<\rho$, we have that $\sin\angle(pq,T_p)\le\frac{\|q-p\|}{2\rho}$, and the distance from q to T_p is bounded by $\frac{\|q-p\|^2}{2\rho}$, where ρ is the local feature size of p, T_p is the tangent plane at p.

***Lemma** 2.3 (Theorem 3.2 in [1]):* Suppose P is an ε-sample of $\mathcal{M}$. For $p \in P$ with local feature size ρ and real tangent plane T_p. Compute $\hat{T}_p$ as in Algorithm PCDLaplace [1], $\angle(T_p, \hat{T}_p) = O(r/\rho)$ for $r < \rho/2$ and $r \geq 10\varepsilon$.

***Lemma** 2.4 (Lemma 1 in [4]):* Given any openset $B \subset \mathcal{M}$, $p \in B$, for any positive natural number l,

$$\int_{B \subset M} e^{-\frac{\|p-y\|}{4t}} f(y) d\mu_y - \int_M e^{-\frac{\|p-y\|}{4t}} f(y) d\mu_y = o(t^l).$$

***Lemma** 2.5 (Lemma 5 in [4]):*

$$\Delta_{\mathcal{M}} f(p) = \lim_{t \to 0} \frac{1}{4\pi t^2} \Big(\int_{\mathcal{M}} e^{-\frac{\|p-y\|^2}{4t}} f(p) d\mu_y - \int_{\mathcal{M}} e^{-\frac{\|p-y\|^2}{4t}} f(y) d\mu_y \Big).$$

3 Lemmas about Voronoi Cells

In this paper we are using the Voronoi cells $Vr_{\hat{T}}(p)$ on the estimated tangent planes $\hat{T}_p$. This appendix section shows some results that are related to Voronoi cells over 2-planes and are used for our convergence proof of Theorem 4.1.

***Lemma** 3.1:* For plane L and point set $P \subset L$, consider the Voronoi diagram of P over L. Let $p \in P$. Suppose the Voronoi cell of p is $Vr(p)$ and the cell boundary is $\partial Vr(p)$. $\forall \tilde{p} \in \partial Vr(p)$, $\|p - \tilde{p}\| \leq \varepsilon$.

If we fix point p and move all the other points $q \in P$ as: $q' = p + (q - p) \cdot t$, $t > 0$, Then the area of the new Voronoi cell $Vr'(p)$ has such property:

$$\frac{\mathrm{vol}(Vr'(p))}{\mathrm{vol}(Vr(p))} = t^2. \tag{3.1}$$

Proof:

Suppose the plane L is parameterized in (u, v) coordinates with p being the origin. For point $q_i \in P$ and corresponding displaced point q_i', we have their coordinate relationship: $(u_i', v_i') = t(u_i, v_i)$.

So we can build the mapping $f : L \to L$ as $m' = f(m) = f(u, v) = (tu, tv)$, where $m, m' \in L$. Thus we have

$$\forall m \in L, \|m' - p\| = t\|m - p\|,$$
$$\forall m \in L, \|m' - q_i\| = t\|m - q_i\|.$$

It's obvious that $m \in Vr(p) \leftrightarrow m' = f(m) \in Vr'(p)$. Then we have

$$\mathrm{vol}(Vr'(p)) = \int_{Vr'(p)} du'dv' = \int_{Vr(p)} t^2 du dv = t^2 \,\mathrm{vol}(Vr(p)).$$

□

***Lemma** 3.2:* Consider plane L and point set $P \subset L$, as defined in Lemma 3.1. If we move one point $q \in P$ as: $q' = p + (q - p) \cdot t$, $0 < t < 1$, then the area of the new Voronoi cell $Vr'(p)$ has such property:

$$\mathrm{vol}(Vr'(p)) \leq \mathrm{vol}(Vr(p)). \tag{3.2}$$

Proof:

Suppose l_{pq} and $l_{pq'}$ are the bisecting planes between the point-pairs $\{p, q\}$ and $\{p, q'\}$. $\forall m \in Vr'(p)$, we have $\|m - p\| < \|m - q'\|$. That is, m resides on the p-side of $l_{pq'}$. As shown in figure 7, it is obvious that $l_{pq'}$ resides on the p-side of l_{pq}. Thus we have $m \in Vr(p)$.

Thus $Vr'(p) \subseteq Vr(p)$. □

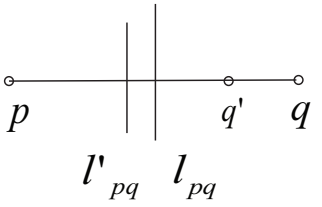

Fig. 7. Moving a point in the Voronoi diagram.

***Lemma** 3.3:* Consider plane L and point set $P \subset L$, as defined in Lemma 3.1. If we fix point p and move all the other points $q \in P$ as: $q' = p + (q - p) \cdot t_q$, $t_q > 0$, then we have the following result about the new Voronoi cell $Vr'(p)$:

$$(\min(t_q))^2 \leq \frac{\mathrm{vol}(Vr'(p))}{\mathrm{vol}(Vr(p))} \leq (\max(t_q))^2. \tag{3.3}$$

Proof: From Lemma 3.2, we know that the area of $Vr'(p)$ will change monotonically with t_q. So combine it with Lemma 3.1 we can get this lemma proved. □

4 Lemmas about Small Angles

This appendix section shows the Lemmas about small angles that we used for the equation (1.22) in the proof of Theorem 4.1.

***Lemma** 4.1 (Angles of 3 Planes):* Consider 3 planes T_1, T_2 and T_3 with their corresponding unit normal vectors $\mathbf{n}_1$, $\mathbf{n}_2$ and $\mathbf{n}_3$. Denote $\angle(\mathbf{n}_1, \mathbf{n}_2) = \alpha$, $\angle(\mathbf{n}_2, \mathbf{n}_3) = \beta$, $\angle(\mathbf{n}_1, \mathbf{n}_3) = \gamma$. Without any loss of generality, assume α, β, γ are all acute angles.

If $\alpha < \pi/4$, $\beta < \pi/4$, then we have $\gamma \leq \alpha + \beta$ holds.

Proof:

Since we are observing 3 unit vectors, it's convenient to put them on unit sphere S, as shown in figure 8 (left). Consider the geodesic distance $g(\mathbf{n}_1, \mathbf{n}_2)$, $g(\mathbf{n}_2, \mathbf{n}_3)$ and $g(\mathbf{n}_1, \mathbf{n}_3)$ on S. It's obvious that all these geodesics are part of great circles of S. From the definition of geodesic distance, we know that $g(\mathbf{n}_1, \mathbf{n}_3) \leq g(\mathbf{n}_1, \mathbf{n}_2) + g(\mathbf{n}_2, \mathbf{n}_3)$. Since S is unit sphere, we also have $g(\mathbf{n}_1, \mathbf{n}_2) = \alpha$, $g(\mathbf{n}_2, \mathbf{n}_3) = \beta$, $g(\mathbf{n}_1, \mathbf{n}_3) = \gamma$. So we have $\gamma \leq \alpha + \beta$ holds. □

***Lemma** 4.2 (Angles of 2 Planes and 1 Vector):* Consider 2 planes T_1 and T_2 with their corresponding unit normal vectors $\mathbf{n}_1$ and $\mathbf{n}_2$. Consider another unit vector $\mathbf{n}_3$. Denote $\angle(\mathbf{n}_1, \mathbf{n}_2) = \alpha$, $\angle(T_2, \mathbf{n}_3) = \beta$, $\angle(T_1, \mathbf{n}_3) = \gamma$.

If $\alpha < \pi/4$, $\beta < \pi/4$, then we have $\gamma \leq \alpha + \beta$ holds.

Proof:

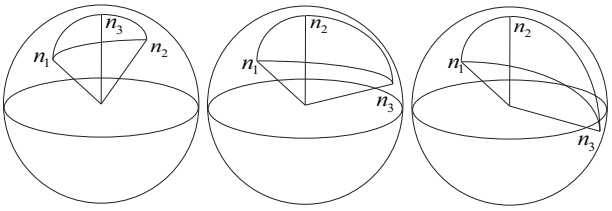

Fig. 8. Unit vectors on the unit sphere: Lemma 4.1 (left) and Lemma 4.2 (middle and right).

Similar to the proof of Lemma 4.1, we put all vectors on the unit sphere S. Select proper $\mathbf{n}_1$ and $\mathbf{n}_2$ directions to ensure that $\mathbf{n}_1 \cdot \mathbf{n}_2 \geq 0$.

In case $\mathbf{n}_2 \cdot \mathbf{n}_3 \geq 0$, as shown in figure 8 (middle), we have $\angle(\mathbf{n}_2, \mathbf{n}_3) = \pi/2 - \beta$. From Lemma 4.1, we know that:

$\angle(\mathbf{n}_1, \mathbf{n}_3) \leq \angle(\mathbf{n}_1, \mathbf{n}_2) + \angle(\mathbf{n}_2, \mathbf{n}_3) = \pi/2 + \alpha - \beta$,
$\angle(\mathbf{n}_1, \mathbf{n}_3) \geq \angle(\mathbf{n}_2, \mathbf{n}_3) - \angle(\mathbf{n}_1, \mathbf{n}_2) = \pi/2 - \alpha - \beta$.

Thus we have $\gamma = \angle(T_1, \mathbf{n}_3) \leq \alpha + \beta$ holds.

In case $\mathbf{n}_2 \cdot \mathbf{n}_3 \leq 0$, as shown in figure 8 (right), we have $\angle(\mathbf{n}_2, \mathbf{n}_3) = \pi/2 + \beta$. Similarly we also have $\gamma = \angle(T_1, \mathbf{n}_3) \leq \alpha + \beta$. □

REFERENCES

[1] M. Belkin, J. Sun, and Y. Wang, "Constructing Laplace operator from point clouds in $\mathbb{R}^d$," in *Proceedings of the 19th Annual ACM-SIAM Symposium on Discrete Algorithms*. Philadelphia, PA, USA: Society for Industrial and Applied Mathematics, 2009, pp. 1031–1040.

[2] K. Hildebrandt and K. Polthier, "On approximation of the laplace-beltrami operator and the willmore energy of surfaces," *Computer Graphics Forum*, pp. 1513–1520, 2011.

[3] K. Hildebrandt, K. Polthier, and M. Wardetzky, "On the convergence of metric and geometric properties of polyhedral surfaces," *Geometriae Dedicata*, vol. 123, no. 1, pp. 89–112, 2006.

[4] M. Belkin and P. Niyogi, "Towards a theoretical foundation for Laplacian-based manifold methods," in *Lecture Notes on Computer Science*. Springer-Verlag, 2005, vol. 3559/2005, pp. 486–500.

[5] M. Belkin, J. Sun, and Y. Wang, "Discrete Laplace operator on meshed surfaces," in *Proceedings of the 24th Annual Symposium on Computational Geometry*. New York, NY, USA: ACM, 2008, pp. 278–287.

[6] J. Giesen and U. Wagner, "Shape dimension and intrinsic metric from samples of manifolds with high co-dimension," in *Proceedings of the 19th Annual Symposium on Computational Geometry*. New York, NY, USA: ACM, 2003, pp. 329–337.